Title: A genome wide CRISPR screen reveals novel determinants of long-lived plasma cell secretory capacity

Authors: Lucas J. D'Souza[1], Jonathan N. Young[2,3], Heather Coffman[2,4], Edward P. Petrow Jr.[5], and Deepta Bhattacharya[1,*]

Affiliations:

[1]Department of Immunobiology, University of Arizona; Tucson, AZ.

[2]Department of Otolaryngology, University of Arizona; Tucson, AZ.

[3]Current Address: Department of Otolaryngology, Sutter Medical Group; Sacramento, CA.

[4]Current Address: Phoenix Indian Medical Center; Phoenix, AZ.

[5]Tucson Orthopedic Institute; Tucson, AZ.

*Corresponding author. Email: deeptab@arizona.edu

Abstract: Plasma cell subsets vary in their lifespans and ability to sustain humoral immunity. We conducted a genome-wide CRISPR-Cas9 screen in a myeloma cell line for factors that promote surface expression of CD98, a marker of longevity in primary mouse plasma cells. A large fraction of genes found to promote CD98 expression in this screen are involved in secretory and other vesicles, including many subunits of the V-type ATPase complex. Chemical inhibition or genetic ablation of V-type ATPases in myeloma cells reduced antibody secretion. Primary mouse and human long-lived plasma cells had greater numbers of acidified vesicles than did their short-lived counterparts, and this correlated with increased secretory capacity of IgM, IgG, and IgA. The screen also identified PI4KB, which promoted acidified vesicle numbers and secretory capacity, and DDX3X, an ATP-dependent RNA helicase, the deletion of which reduced immunoglobulin secretion independently of vesicular acidification. Finally, we report a plasma-cell intrinsic function of the signaling adapter MYD88 in both antibody secretion and plasma cell survival *in vivo*. These data reveal novel regulators of plasma cell secretory capacity, including those that also promote lifespan.

One Sentence Summary: Long-lived plasma cells rely on V-type ATPases, PI4K, DDX3X, and MYD88 signals for maximal secretory capacity

Main Text:

INTRODUCTION

The humoral response following infection or vaccination involves recognition and activation of B cells by cognate antigen, followed by expansion, selection, and differentiation of these cells into quiescent memory B cells and antibody secreting plasma cells. If these antibodies are specific for protective epitopes on the pathogen, even small quantities can protect against otherwise lethal infections (*1*). Thus, maintenance of protective antibody production is a key aspect of durable immunity. Yet, antibody production following some vaccines and infections are stable over time whereas others do so more transiently (*2–5*). Underlying this variability are the numbers and lifespans of plasma cells that are generated.

Plasma cell subsets of varying longevity can be distinguished by a combination of various phenotypic markers. Human long-lived plasma cells tend to lack expression of CD19 (*6*, *7*), though there are some exceptions to this rule (*8*, *9*). In mice, a combination of markers such as BLIMP1 expression, B220, CD93, CXCR3, MHC-II, SLAMF6, LAG3, and the uptake of the fluorescent compound 2-deoxy-2-[(7-Nitro-2,1,3-benzoxadiazol-4-yl)-amino]-D-glucose (2NBDG) define plasma cell subsets of varying lifespans (*10–13*). Another marker is the solute carrier protein CD98, which on the cell surface is subtly more highly expressed by long-lived plasma cells relative to their shorter-lived counterparts (*12*). CD98 is a heterodimer is comprised of a heavy chain encoded by the *Slc3a2* gene and a light chain by the *Slc7a5* gene (*14*). This covalent pairing is not exclusive as the SLC3A2 protein can pair with other members of the SLC7 family to form a variety of transporters involved in amino acid uptake (*15*). Besides

importing amino acids, CD98 can also interact with integrin β subunits to facilitate cell growth and survival (*16*). In plasma cells, the transcription factor BLIMP1 directly binds at the *Slc7a5* locus and promotes its expression (*17*).

The activity of BLIMP1 is a major defining factor for inducing antibody secretory capacity in plasma cells. It does so in three distinct ways: first, by inducing a robust increase in transcription of *Igh* and *Igl* transcripts in plasma cells (*18*); second, by upregulating the elongation factor ELL2 that permits alternative processing of the 3' end of *Igh* transcripts and enabling translation of secretion-specific immunoglobulin heavy-chain proteins (*19*); and lastly by inducing ATF4, ATF6, and XBP1 expression to support the high rate of antibody synthesis and folding as well as expansion of the ER network and secretory apparatus necessary for secretion (*17*, *20–23*). Aside from BLIMP1, mTORC1 signaling is another key pathway that promotes antibody secretion (*24–26*).

There is conflicting evidence of whether antibody secretory capacity and plasma cell lifespan are related or independent. On one hand, deletion of the transcription factor XBP-1 sharply reduces antibody secretory capacity but does not impact plasma cell differentiation or survival (*23*). Similarly, genetic ablation of mTOR signaling in plasma cells reduces secretory capacity but not survival (*24*). These data demonstrate that there is no absolute requirement of antibody secretion for plasma cell survival. On the other hand, long-lived plasma cells tend to secrete more antibodies on a per cell basis than do their short-lived counterparts, but expression of XBP-1 and mTOR signaling are similar across these subsets (*12*). It therefore remains possible that some pathways link lifespan and secretory capacity, perhaps explaining some of the functional

heterogeneity in plasma cells. To identify such pathways, we performed an unbiased loss-of-function screen for genes that promote CD98 expression in plasma cells and investigated their roles in plasma cell function and longevity.

RESULTS

CD98 expression on plasma cells correlates with 2NBDG uptake and is independent of secreted antibody isotype

We first characterized markers of plasma cell longevity that could potentially be used in genome-wide CRISPR screens. In previous work, we showed that 2NBDG uptake correlated with the longevity of plasma cell subsets (*10*, *12*). Plasma cells that were 2NBDG+ also showed slightly higher levels of the large neutral amino acid transporter CD98, which is composed of SLC3A2 and SLC7A5, relative to their 2NBDG- counterparts. To test if immunoglobulin isotype usage impacts these correlations, we injected C57BL/6 (B6) mice with 2NBDG and enriched for CD138+ cells from their spleens and bone marrows. A large fraction of splenic CD138+ B220+/- plasma cells were IgM+ while IgA+ plasma cells made up less than 10% of the pool **(Fig. S1A)**. Consistent with previous reports and in contrast to the spleen (*27*), bone marrow plasma cells were mostly IgM+ or IgA+ **(Fig. S1B)**. IgA+ plasma cells showed the highest frequency of 2NBDG+ cells followed by IgM+, and IgG+ or IgE+ plasma cells in both spleen and bone marrow **(Fig. S1C)**. When matched for antibody isotype, surface CD98 mean fluorescence intensity (MFI) was higher in plasma cells that took up 2NBDG (LLPCs) relative to plasma cells that were 2NBDG- (SLPCs) **(Fig. 1A-C)**. Bone marrow LLPCs showed higher CD98 levels relative to their splenic counterparts. To quantify total, rather than just surface CD98 protein levels, we purified SLPCs and LLPCs from the spleens and bone marrows of B6 mice and examined for expression of CD98 following fixation and permeabilization. Again, bone marrow LLPCs had the highest expression of CD98, followed by splenic LLPCs and then splenic SLPCs **(Fig.**

1D). Consistent with these findings, we used imaging flow cytometry to observe CD98 on both the surface and within the cytosol of fixed and permeabilized plasma cells in all groups **(Fig. 1E)**. Bone marrow LLPCs showed the highest levels of CD98 on their surface as measured by similarity morphology indexes with CD138 as compared to both splenic plasma cell populations **(Fig. 1E)**.

Transcript abundances of *Slc3a2* and *Slc7a5*, as measured by RNAseq (*12*), were similar across plasma cell subsets **(Fig. 1F)**. Further, transcript reads of *Prdm1* which encodes for BLIMP-1, a known regulator of CD98 levels in plasma cells (*17*, *28*), were similar between short- and long-lived subsets **(Fig. 1G)**. Thus, the differences between CD98 expression are apparent across plasma cell subsets irrespective of isotype and do not appear to be regulated at the level of transcription.

A genetic screen to identify factors required for CD98 expression

In prior CRISPR approaches, we were unsuccessful in identifying genes that promote 2NBDG uptake (*13*). Given that elevated CD98 also marks long-lived plasma cell subsets, we carried out an unbiased genome wide CRISPR knockout screen for genes that promote its expression. We engineered the mouse myeloma cell line, 5TGM1, to express a Doxycycline inducible version of Cas9 (5TGM1-iCas9) **(Fig. 2A)**. This strategy was chosen to allow for expansion of cells containing gRNAs that target essential genes which might otherwise have been lost in a constitutive Cas9 expression system. We then transduced 5TGM1-iCas9 cells with the Brie library containing 78,637 gRNAs targeting 19,674 genes of the mouse genome (*29*). After transduction, gRNAs were represented at levels similar to the input plasmid library (r^2=0.57, **Fig. 2B)**. We

induced Cas9 expression by adding Doxycycline to the cell culture media and incubated cells for 7 days to ablate genes and promote complete depletion of residual proteins. From the Doxycycline treated cultures, we then sorted cells with reduced CD98 expression by FACS to purities >95% **(Fig. 2C)**. Genomic DNA was then extracted from these cells and gRNA sequences amplified by PCR from the CD98-low and the total 5TGM1-iCas9-Brie populations. The resultant amplicons were sequenced and the abundance of enriched gRNAs was quantified relative to the total cell fraction using the Model-based Analysis of Genome-wide CRISPR/Cas9 Knockout (MaGeCK) algorithm (*30*).

In the CD98-low fraction, we observed 34 genes targeted by the gRNAs with greater than 2-fold enrichment and with a false discovery rate <0.05 **(Fig. 2D)**. We observed enrichment of gRNAs targeting *Slc3a2* and *Slc7a5*, the genes that encode the heavy and light chains of the CD98 heterodimer, providing internal validation of the results of the genome-wide screen. Among the remaining 32 gRNA-targeted genes, we found 8 genes that associate with endosomal vesicles and 8 members of the vesicle-associated V-type ATPase complex. The remaining 16 genes include those that encode RNA export and processing proteins (*Thoc3*, *Ddx3x*, *Nob1*, *RnaseK*, and *Rbm33*), signaling intermediates (*Myd88*, *Myc*, and *Pi4kb*), proteins involved in genome structure (*Rad21* and *Smc3*), and the chaperone *Hsp90b1*. We were surprised to not have identified *Prdm1* as a hit given its role in promoting CD98 expression (*17*). Yet when we compared cells treated with Doxycycline to untreated controls at day 7, we observed a drop in the read counts for gRNAs targeting *Irf4*, *Prdm1*, *Xbp1*, *Atf4*, and *Atf6b*,

indicating a selection against cells that deleted these genes and potentially limiting their detection in our screen **(Fig. S2)**.

Long-lived plasma cells have higher frequencies of acidic vesicles than do short-lived plasma cells

Given the enrichment of genes involved in multiple vesicular components and V-type ATPases in the screen, we chose to focus on these pathways first. The V-type ATPase is a multi-protein complex made up of a membrane bound proton pump (V0) powered by a cytosol-facing subunit (V1) that hydrolyses ATP (*31*). It acidifies lysosomes, endosomes, Golgi complexes, and secretory vesicles, all of which have significantly lower luminal pH relative to the cytosol (*32*). We purified mouse plasma cell subsets by FACS and examined for the frequencies of acidic vesicles using intracellular staining and imaging cytometry. Total ATP6V1A+ spot numbers per cell were slightly higher in bone marrow LLPCs relative to splenic LLPCs and SLPCs **(Fig. 3A)**. To identify vesicular content differences more specifically between plasma cell subsets we used characteristic markers. RAB7+ endosomes were present at higher frequencies in LLPCs of both spleen and bone marrow compared to SLPCs **(Fig. 3B)**. Further, LAMP1+ lysosome frequencies per cell were highest in bone marrow LLPCs, followed by splenic LLPCs and SLPCs **(Fig. 3C)**. We next examined if human plasma cell populations demonstrated similar trends for endosome and lysosome frequencies (gated as in **Fig. S3**). We observed higher frequencies of ATP6V1A+ and LAMP1+ vesicles in bone marrow plasma cells relative to tonsillar plasma cells **(Fig. 3D-E)**. Put

together, the frequencies of acidic vesicles in plasma cells are higher in subsets with longer lifespans.

We reasoned that these differences in vesicular content might reflect differential antibody secretory capacities of plasma cell subsets. We sorted total SLPCs and LLPCs from the spleens and bone marrows of mice and seeded equal numbers for ELISpot assays, as spot size can serve as a surrogate of antibody secretory capacity (*24*). We found that bone marrow LLPCs yielded spots with the largest average area as compared to its splenic equivalents irrespective of antibody isotype **(Fig. 4A-D)**. Splenic SLPCs spots were the smallest in comparison. Similarly, irrespective of isotype, we found that human CD19- bone marrow plasma cells secreted more antibodies per cell than did CD19+ bone marrow plasma cells which on an average have shorter lifespans than their CD19- counterparts **(Fig. 4E-H)**. These findings suggest that for both mice and humans and across isotypes, long-lived plasma cells have higher numbers of acidic vacuoles and secrete more antibodies than their shorter-lived counterparts.

Ablation of V-type ATPase function reduces antibody secretion

We next addressed if there were a direct link between vesicular pH and the antibody secretion capacity of plasma cells. In the first approach, we chemically inhibited V-type ATPase activity using Bafilomycin A1 (*33*). To detect changes in vesicular pH in cells, we transduced Cas9-expressing 5TGM1 cells (5TGM1-Cas9) with the pH Lysosomal Activity Reporter (pHLARE)-encoding lentivirus (*34*). The resultant 5TGM1-Cas9-pHLARE cells express *R. norvegicus* LAMP1 as a fusion protein with the pH-sensitive superfolder GFP (sfGFP) in the lumen of the lysosome and the pH-

insensitive mCherry on the cytosol side of the lysosome, allowing for ratiometric calculation of lysosomal pH (*35*). We observed a 1.3- to 5.6-fold increase in the ratio of sfGFP to mCherry in these cells with increasing concentrations of Bafilomycin A1 **(Fig. 5A)**. Reciprocally, the MFI of surface CD98 was proportionally reduced in all groups treated with Bafilomycin A1 **(Fig. 5B)**. Culture supernatants from groups treated with higher doses of the inhibitor showed reduced antibody levels relative to untreated controls **(Fig. 5C)**. Lastly, we treated purified plasma cell subsets with this inhibitor and observed a reduction in the spot size of secreted immunoglobulin per cell **(Fig. 5D)**. These findings indicate that pharmacological inhibition of V-type ATPase activity impairs both surface CD98 expression and antibody secretion.

We confirmed these findings genetically by ablating V-type ATPase activity in cells using CRISPR-Cas9. We targeted *Atp6v0b* and *Atp6v1a* as representative genes of the V0 and V1 subunit of the ATPase complex. Targeting these genes led to a nearly two-fold increase in the ratio of sfGFP to mCherry relative to a control gRNA targeting the *Rosa26* locus, indicating a rise in lysosomal pH **(Fig. 5E)**. This increase in sfGFP fluorescence can be traced to increased sfGFP intensity on mCherry+ spots in cells as observed by imaging cytometry **(Fig. 5F)**. In both cases, we observed a drop in surface CD98 levels as well as secreted antibodies in their culture supernatants **(Fig. 5G-H)**. Further, the survival of *Atp6v0b*- and *Atp6v1a*-deficient myeloma cells in culture was compromised relative to control cells **(Fig. S4)**. In conclusion, V-type ATPases promote CD98 expression, survival, and antibody secretory capacity of plasma cells.

***Pi4kb* is essential for vesicular acidification and antibody secretion in plasma cells**

Among the gRNAs enriched in the CD98-low fraction were those targeting *Pi4kb*, the gene that encodes the enzyme phosphatidylinositol-4-hydroxide kinase B **(Fig. 2D)**. It is a type-III PI4K that catalyzes the formation of phosphoinositide-4-phosphate (PI4P) at Golgi surfaces which subsequently feeds vesicle formation (*36–38*). We ablated *Pi4kb* expression in 5TGM1-Cas9 cells using CRISPR-Cas9 and observed reduced numbers of ATP6V1A+ spots per cell as well as LAMP1+ lysosomes per cell **(Fig. 6A-B)**. Deletion of *Pi4kb* in 5TGM1-Cas9-pHLARE cells showed lysosomes with higher sfGFP signal, suggesting that loss of PI4KB impairs vesicular acidification **(Fig. 6C)**. *Pi4kb*-deficient 5TGM1 cells also showed reduced surface CD98 expression, secreted fewer antibodies, and had poor survival in culture **(Fig. 6D-E, S4)**.

DDX3X affects antibody secretory capacity of plasma cells independent of vesicular acidification

gRNAs targeting the ATP-dependent DEAD-box RNA helicase *Ddx3x* were also highly enriched in the CD98-low fraction **(Fig. 2D)**. The DDX3X protein associates with complex secondary structures in mRNA and enables protein synthesis (*39–41*). Deletion of *Ddx3x* in 5TGM1-Cas9 cells resulted in reduced surface CD98 levels and decreased secreted immunoglobulin in culture supernatants **(Fig. 7A-B)**. Ablating *Ddx3x* expression in 5TGM1-Cas9-pHLARE cells did not affect lysosomal pH levels, suggesting that it regulates the antibody secretory capacity of cells thorough a mechanism distinct from the PI4KB-V-type ATPase pathway **(Fig. 7C)**. *Ddx3x*-deficient

myeloma cells also survived poorly in culture over time **(Fig. S4)**. We next lentivirally transduced 5TGM1-Cas9 cells with wild-type human DDX3X (hsDDX3X) or versions with point mutations in their helicase domain (T323I, R326H) or aberrations in their ATP-binding domain (I415Δ, T532M) that have previously been reported in patients with DDX3X syndrome (*42*). We then depleted murine wild-type DDX3X in these cells using a gRNA that targets mouse *Ddx3x* but not the transgenic hs*Ddx3x* cassette. At 5 days post-transduction, we found that deleted cultures were rescued by unmodified hsDDX3X (WT) as measured by surface CD98 levels **(Fig. 7D-E)**. When quantified by ELISA, these cultures also showed similar levels of secreted immunoglobulin in their supernatants relative to untargeted control cells, indicating that expression of hsDDX3X overcame the defect otherwise seen with ablation of endogenous DDX3X **(Fig. 7F)**. In all cases, overexpression of hsDDX3X mutants failed to rescue surface CD98 levels or secreted immunoglobulin in culture supernatants **(Fig. 7D-F)**. This observation is not because of differential levels of DDX3X overexpression, as they were found to be comparable across all groups when probed for intracellular DDX3X protein **(Fig. S5)**. Thus, both the ATPase and helicase domain of DDX3X are necessary for proper CD98 expression and antibody secretion in plasma cells.

MYD88 is a plasma cell intrinsic determinant of antibody secretion capacity

We observed an enrichment of gRNAs targeting the signaling intermediate MYD88 in the CD98-low fraction **(Fig. 2D)**. MYD88 is an adaptor protein required for transducing signals through all Toll-like receptors (TLRs), the IL-1 receptor (IL-1R), and cytokine signals through Transmembrane Activator and CAMI Interactor (TACI) by

TRAF6-dependent and -independent mechanisms (*43*). As *Myd88*-knockout (KO) mice are viable and do not show any defects in B cell development (*44*), we first examined plasma cell subsets for CD98 expression and antibody secretion. We injected *Myd88*-KO and age- and sex-matched C57BL/6N mice with 2NBDG and purified plasma cell subsets from the spleens and bone marrows of these mice. We then seeded equal numbers of these cells into an ELISpot assay. As signals downstream of MYD88 promote class-switch recombination (*45*), we compared only IgM-expressing plasma cell subsets. Across all 2NBDG-subsets, *Myd88*-KO plasma cells had lower expression of surface CD98 **(Fig. 8A)**. IgM+ spot areas were reduced only in splenic and bone marrow LLPCs, suggesting that MYD88 signals promote antibody secretion in longer-lived plasma cell subsets **(Fig. 8B)**.

To test if MYD88 affects antibody secretory capacity in a plasma cell intrinsic manner, we generated lineage specific *Myd88* knockout mice. We bred mice with loxP sites flanking exon 3 of the *Myd88* genomic locus (*Myd88* fl/fl) with mice carrying an IRES-CreERT2 cassette at the 3' UTR of the *IgJ* locus (Jchain-CreERT2). In these mice, treatment with tamoxifen induces deletion of *Myd88* in plasma cells (*46*, *47*), allowing for assessment of its function independently of other factors altered in germline knockout mice, such as the microbiome. We immunized these mice (Jchain-CreERT2+/- *Myd88* fl/fl) along with littermate Cre-negative (Jchain-CreERT2-/- *Myd88* fl/fl) and Cre-only (Jchain-CreERT2+/-) control mice with 100µg NP-CGG in 1% Alhydrogel, an adjuvant that does not activate TLR signals (*48*). At 8 weeks, we observed comparable levels of serum NP-specific antibodies across all groups **(Fig. 8C)**. We then fed mice Tamoxifen chow over the course of 2 weeks to induce deletion of *Myd88*. Bone marrow

287 LLPCs from these treated mice were then enriched and examined for spot frequencies
288 and sizes in ELISpot assays. We observed a significant reduction in both the numbers
289 and spot sizes of NP-specific plasma cells in the bone marrows of Jchain-CreERT2+/-
290 *Myd88* fl/fl mice relative to both control mouse groups **(Fig. 8D-E)**. This suggests that
291 plasma cell intrinsic MYD88 signaling promotes both survival and secretory capacity of
292 plasma cells.

293 Finally, to identify candidate pathways through which MYD88-dependent signals
294 promote antibody secretion, we examined previously generated RNAseq databases for
295 expression of receptors that signal through MYD88 in plasma cells and 5TGM1 cells
296 (*12*, *13*). *Il1r* transcripts were undetectable in all populations examined, but expression
297 of *Tnfrsf13b*, the gene that encodes TACI, was readily observed in all groups **(Fig.
298 S6A).** Though primary plasma cells did express several TLR family members, 5TGM1
299 cells only expressed *Tlr4* **(Fig. S6B)**. We therefore ablated *Tnfrsf13b*, *Tlr4*, *Myd88*, and
300 *Traf6* (the gene that encodes TRAF6, a downstream molecule of the MYD88 cascade)
301 in 5TGM1 myeloma cells using CRISPR-Cas9. We found that ablation of each of these
302 genes resulted in reduced surface CD98 and fewer antibodies secreted in culture
303 supernatants relative to cells transduced with a control gRNA targeting the *Rosa26*
304 locus **(Fig. 8F-G)**. These data suggest that signaling through TACI and perhaps by
305 endogenous TLR4 ligands via MYD88 may promote the antibody secretory capacity of
306 plasma cells.
307

DISCUSSION

Plasma cell subsets vary in their lifespans and presumably their ability to sustain durable humoral immunity. Subtle differences in CD98 expression distinguish these subsets, thereby providing a convenient handle for unbiased genome-wide screens for factors that promote plasma cell longevity. We identified 34 genes that included a variety of vesicular proteins, subunits of the V-type ATPase complex, RNA export and processing proteins, and various signaling intermediates that promote CD98 expression. Though the original intent of the screen was to identify determinants of lifespan, most of the identified factors also or exclusively impacted secretory capacity. These data suggest some convergence in factors that fine tune plasma cell lifespan and antibody secretion.

Nearly half of the genes identified in our screen encode proteins associated with intracellular vesicles and vesicular acidification. These organelles are relevant to plasma cells as a properly functioning secretory network is crucial to support the high rate of translation, folding, and secretion of antibodies in these cells (*32*). We observed the frequency of acidic vacuoles to be higher in longer-lived plasma cell subsets, consistent with their elevated antibody secretory capacity relative to their short-lived counterparts. Impeding RAB7 exchange with RAB5 on endosomes inhibited antibody secretion and plasma cell longevity, demonstrating the importance of endosomal function in plasma cells (*49*, *50*). The greater numbers of acidic vesicles in long-lived plasma cells compared to short-lived plasma cells likely depend on the activity of the inositol kinase PI4KB, which has been shown in multiple systems to promote lysosomal integrity, vesicle formation, and retention of integral proteins to these organelles like the

V-type ATPase complexes (*51*, *52*). The factors that might promote differential PI4KB activity in plasma cell subsets are currently unknown.

Our data further reveals the complex regulation of antibody secretion in plasma cells by identifying a role for the RNA helicase DDX3X in modulating this process. This protein has been shown to associate with secondary structures at the 5' end of mRNA and unwinds them through its helicase activity, allowing for recruitment of ribosomes and its subsequent translation (*41*, *53*). In plasma cells, this function is particularly relevant as DDX3X activity might ease barriers in mRNA translation and support a steady rate of antibody synthesis and secretion. While it is likely that DDX3X associates with *Igh* and *Igl* mRNA due to their sheer abundance in plasma cells, identifying transcripts bound to DDX3X in plasma cells might provide insights to the translational regulation of key proteins for cellular function. As mice with lymphocyte-specific ablation of *Ddx3x* show reductions in B cell numbers (*54*, *55*), generating inducible models of *Ddx3x* deletion may help us understand the role of this factor in plasma cell longevity. Further, as males express a homolog of DDX3X called DDX3Y, it would be interesting to observe if the two factors have overlapping targets in plasma cells from males and compensate for each other in the absence of one or the other (*56*).

While MYD88 has been well-studied in B cells, our report demonstrates a plasma cell-intrinsic role for this signaling intermediate in modulation CD98 expression, survival, and antibody secretion. MYD88 may act through TACI, a receptor for BAFF and APRIL, cytokines with known roles in plasma cell survival (*57*, *58*). Signals through this cytokine-receptor pair are particularly relevant in the bone marrow niche, where plasma cells are immersed in a milieu of extracellular matrix proteins, cytokines, and cell

adhesion factors that promote their survival *in vivo* (*59–62*). MYD88 is also a key adaptor downstream of most TLRs and is crucial for signal transduction following PAMP recognition. *In vivo* plasma cells may have TLR signaling induced by low concentrations of circulating PAMPs that stimulate intracellular or surface TLRs. As the myeloma cells are cultured free of TLR ligands and cytokines, MYD88 signaling is likely induced by endogenous TLR ligands like HMGB1 following cell death *in vitro* (*63*). Our findings offer evidence that in addition to promoting plasma cell survival, signals through MYD88 also influence the antibody secretory capacity of cells, offering yet another link between lifespan and function in plasma cells. The data also indicates that the secretory capacity of plasma cells is not exclusively a cell-intrinsic function but can be modulated by external stimuli.

CRISPR-Cas9 screens were recently carried out by multiple independent groups to identify factors regulating plasma cell differentiation (*64*, *65*) and antibody secretion (*66*) using *in vitro* primary B cell systems. Of the genes shown to be important for antibody secretion in these studies, such as those involved in the unfolded protein response, we found little overlap with the genes in our dataset. This may be due to our use of CD98 as a marker, which varies with antibody secretory capacity across plasma cell subsets but not as a function of the unfolded protein response (*12*). Our screen was thus more likely to identify pathways that differ subtly between plasma cell subsets rather than those that are central components of the secretory machinery. Put together, our data suggest there are distinct programs required for the induction of antibody secretion: those that are absolutely required and used similarly across plasma cell subsets, and others that further tune lifespan and secretory capacity. At least some of

the latter pathways functionally link survival and antibody secretion, thereby allowing relatively few highly secretory long-lived plasma cells to provide robust protection.

MATERIALS AND METHODS

Study design

To identify genes and pathways regulating CD98 expression, we FACS-sorted Doxycycline treated 5TGM1-iCas9 cells transduced with the mouse Brie library that had reduced expression of surface CD98. Of the various hits, we investigated the role of V-type ATPases, PI4KB, DDX3X, and MYD88 as key regulators of CD98 expression, antibody secretory capacity, and longevity. Intracellular acidic vacuole spot numbers were quantified from *ex vivo* plasma cells using imaging flow cytometry. Vesicular acidity in myeloma cells following gene ablation were assessed using a lysosome-specific pH-sensitive GFP and flow cytometry. Antibody secretion from *ex vivo* IgM+, IgG+, and IgA+ plasma cells was done by ELISpot assays while secretion in edited myeloma cells done by ELISA of culture supernatants. Human DDX3X and mutants were overexpressed in myeloma cultures followed by deletion of endogenous mouse DDX3X using CRISPR-Cas9 and evaluation of antibody secretion. We generated plasma cell specific *Myd88* knockout mice and assessed for plasma cell survival and function after tamoxifen treatment by ELISA and ELISpot assays. Statistical analysis was carried out using Prism.

Mice

C57BL/6N mice (556) were purchased from the Charles River laboratories. *Myd88*-null (9088) and *Myd88*-flox (8888) mice were purchased from Jackson Laboratories (*46*). Jchain-CreERT2 mice have been generated previously (*47*). Mice were housed and bred under specific pathogen free conditions. Experiments were carried out on age- and sex-matched mice between 8-12 weeks in age. All animal procedures were executed

403 under the guidelines provided by the Institutional Animal Ethics committee of the
404 University of Arizona. Euthanasia was carried out by carbon dioxide asphyxiation at the
405 rate of 1.8-4.0 L/minute in a 7L chamber until 1 minute after respiration ceased. Mice
406 were then cervically dislocated to ensure death. For some experiments, mice sedated
407 with Fluriso (Vet One) were injected intravenously with 100µg of 2NBDG (Cayman
408 Chemical company) and euthanized after 20 minutes.

409 ***Human tissues***

410 Tonsil samples were obtained from adults undergoing elective tonsillectomies (Banner-
411 University Medical Center). Tonsils were extracted from anesthetized individuals using
412 Bovie electrocautery in a standard tonsillectomy surgery. Bilateral tonsils were
413 subsequently combined and provided as a fresh sample for processing to the lab with
414 age and sex as the only associated information. Bone marrow reaming samples were
415 obtained from individuals undergoing robotics-assisted hip arthroplasty (Tucson
416 Orthopedic Institute). All bone marrow donors were anonymous, and no patient data
417 was collected as part of this investigation. The Human Research Protections Office of
418 the University of Arizona and the Banner Health Non-Research Data Use Committee
419 classified both studies as 'non-human subjects' research.

420 ***Immunizations***

421 Mice were immunized intraperitoneally with 100µg NP-CGG (Biosearch Technologies)
422 in 1% Alhydrogel (Invivogen). Circulating blood was collected by venipuncture of the tail
423 vein from immunized mice and allowed to stand at room temperature to coagulate
424 overnight. Serum was collected after spinning down the samples at 15000rpm for 10

minutes. At 8 weeks post-immunization, mice were fed special chow containing 400mg Tamoxifen citrate per kg diet (Envigo) for two weeks prior to euthanasia.

Primary cells

Single cell suspensions of spleens were prepared by macerating organs with frosted slides while bone marrow cells were isolated from tibiae, fibulae, femurs, and pelvic bones using a mortar and pestle in 1x PBS containing 5% Adult bovine serum (MP Biomedical; hereon referred to as FACS buffer). Human tonsils were sliced using a scalpel and forceps and ground in FACS buffer using a mortar and pestle. Human bone marrow reamings were shaken vigorously in a sterile container containing FACS buffer. In all cases, cells were filtered through a 70-micron nylon mesh to remove debris. Single cell suspensions were treated in an ammonium chloride-potassium (ACK) hypotonic lysis solution to lyse erythrocytes followed by density gradient centrifugation on a Histopaque-1119 layer (Millipore Sigma). To enrich for murine plasma cells, whole cell suspensions were enriched by labelling with an appropriate anti-CD138 antibody (Biolegend) followed by anti-APC or anti-PE microbeads and enriched using LS columns (all from Miltenyi Biotec). CD38+ tonsil and bone marrow cells were enriched similarly from whole cell suspensions. For some experiments, CD38-enriched cells were cryopreserved in 50% incomplete RPMI (Thermo Fisher Scientific), 40% fetal calf serum (Peak Serum), and 10% DMSO (Millipore Sigma) until the time of experimentation. For intracellular staining, cells were first fixed with 2% Paraformaldehyde (Electron microscopy services) for 10 minutes followed by permeabilization with 0.1% Saponin (Millipore Sigma).

Plasmids

The mouse Brie CRISPR-knockout library (73633), lentiGuide-puro (52963), pLenti-sfGFP-LAMP1-mCherry (164478), and pHAGE-DDX3X (116730) were all purchased from Addgene (*29*, *34*, *67*, *68*). The lentiGuide-mCherry plasmid (217005) was generated in-house (*13*). Edit-R inducible lentiviral hEF1α-Blast-Cas9 nuclease plasmid (CAS11229) was purchased from Dharmacon. Guide RNA (gRNA) targeting genes of interest were chosen from the Brie CRISPR-knockout library and cloned into an empty lentiGuide-puro construct as described previously (*13*). Mouse genomic *Ddx3x*-specific gRNA were designed using CRISPick (*29*, *69*). pMD2.G (12259) and psPAX2 (12260) were used to generate lentivirus and were also purchased from Addgene. T323I, R326H, I415Δ, and T532M mutations were introduced into the parental pHAGE-DDX3X by PCR and site-directed mutagenesis using the KLD enzyme reaction (New England Biolabs). Positive mutants were identified by Sanger sequencing (Eton Biosciences). Plasmids were transformed and grown in XL-1 Blue cells (Agilent Technologies) or *Stbl4* competent cells (Thermo Fisher Scientific) for plasmids larger than 10kb.

Cell lines and cell culture

The 5TGM1 myeloma line was a gift from Michael H. Tomasson (*70*). 5TGM1 cells expressing a Doxycyline-inducible Cas9 (5TGM1-iCas9) was generated by transducing cells with lentivirus containing the Edit-R inducible Cas9 construct at 2500rpm for 90 minutes at room temperature followed by culturing cells in media containing 10µg/mL Blasticidin-HCl (Thermo Fisher Scientific). Cells were sorted into single cell clones by FACS and screened for lines not expressing Cas9 in regular doxycycline-free media. 5TGM1 cells expressing Cas9 constitutively (5TGM1-Cas9) were generated previously (*13*). These cells were transduced with lentivirus containing the pHLARE cassette by

spin-infection and positive cells were FACS-sorted as GFP+ mCherry+ cells. Overexpression constructs for human DDX3X and mutants were introduced into 5TGM1-Cas9 cells similarly and purified based on GFP expression. All 5TGM1 lines were cultured in RPMI (Gibco) containing 10% FBS, 1mM Sodium pyruvate, 2mM GlutaMAX, 10µg/mL Ciprofloxacin-HCl, minimum-essential amino acids, Penicillin and Streptomycin (hereon referred to as cRPMI). After introduction of gRNA constructs, cells were incubated for 5 days at 37°C with 5% CO_2. For antibody secretion assays, 100,000 5TGM1 cells were seeded in triplicates into wells of a 96-well plated and incubated overnight. Culture supernatants were harvested the next day and assayed for secreted immunoglobulins. Where indicated, cells were treated with Bafilomycin A1 (Millipore Sigma) at varying concentrations. Lenti-X 293T cells (Takara) were cultured in DMEM (Cytiva) with all the additional supplements described previously for RPMI. Lentivirus were generated from these cells by transient transfection of plasmids with packaging constructs previously complexed with GeneJuice (Millipore Sigma).

Flow cytometry

Single cell preparations were stained with the following antibodies from Biolegend: anti-mouse CD138-PE, -APC, or -BV510 (281-2); anti-mouse B220-AlexaFluor700 (RA3-6B2); anti-mouse CD98-AlexaFluor647 or -PE-Cy7 (RL388); anti-human CD38-PE (HB-7); anti-human CD27-APC (M-T271); anti-human CD19-BV421 (HIB19); anti-human IgM-BV650 (MHM-88); anti-human CD138-FITC (MI15). Rat anti-mouse IgA-BV421 (C10-1) was purchased from BD Biosciences. Goat F(ab')2 anti-human IgA-AlexaFluor647 (2052-31) was purchased from Southern Biotech. Unconjugated antibodies against mouse/human ATP6V1A (EPR19270), RAB7 (EPR7589), and

LAMP1 (ab24170) were all purchased from Abcam and used at a 1:500 dilution. Stained organelles were detected with an anti-rabbit IgG-AlexaFluor405 reagent (A48258, Thermo Fisher Scientific). Other antibodies from Thermo Fisher Scientific used in this study are anti-mouse IgM-PerCP-eFluor710 (II41), and anti-mouse/human DDX3X (A300-474A). Propidium iodide and DAPI (both from Millipore Sigma), were used to stain dead cells in some assays. In some experiments Zombie UV or Zombie Red (both from Biolegend) were used to stain dead cells prior to fixation and permeabilization. Cells were analyzed for fluorescence on a BD Fortessa cytometer (BD Biosciences) and data interpreted using the FlowJo software (BD Biosciences). Intracellular organelle frequencies in cells were examined on an Imagestream^{X} MkII (Cytek Biosciences) at 60x magnification with extended depth of field. Spot numbers per cell and similarity morphology indexes were calculated on the IDEAS software (Cytek Biosciences). Fluorescence associated cell sorting was carried out on a FACS Aria II (BD Biosciences).

Library screening and next generation sequencing

The mouse Brie library was packaged into lentiviral particles by transient transfection of Lenti-X 293T cells with the 5µg of the library plasmid, 1.75µg of pMD2.G and 3.25µg of psPAX2 packaging constructs complexed with the GeneJuice transfection reagent (Millipore Sigma). Culture supernatants were collected and pooled at 48h and 96h and filtered through a 0.45µ syringe filter. Fresh filtered supernatants containing virus were then used to transduce 5TGM1-iCas9 cells in the presence of 8µg of Polybrene (Millipore Sigma). Positively transduced cells were then selected in cRPMI containing Puromycin (Gibco). Cas9 expression in 40 million positively transduced 5TGM1-iCas9

cells (roughly 500x coverage of plasmid library) was induced after adding 300ng/mL Doxycycline hyclate to culture media. After 7 days, cells were cultured with 10µg/mL of 2NBDG and then stained for surface CD98 expression. Live CD138+ CD98-low cells were then FACS sorted into individual 15mL conical tubes. Genomic DNA from cells were extracted using the mini genomic DNA extraction kit (IBI scientific) and gRNA constructs amplified using Q5 Polymerase (New England Biolabs). Flow cell attachment sequences, Illumina sequencing regions, and unique 3' barcode sequences were then introduced by PCR. These pair-ended 150bp libraries were then sequenced on a Novaseq 6000 (Illumina). FASTQ files containing 325-926 million reads were then analyzed for gene enrichment in sorted fractions using the Python-based MaGeCK module (*30*). Representation of the Brie library in cells were confirmed by comparing representation of gRNA from positively transduced cells to the parental Brie library. Volcano plots showing enriched genes in sorted fractions relative to unenriched cells were plotted using Prism v.10 (Graphpad).

ELISA

ELISA plates (Corning) were coated overnight at $4^{O}C$ with unconjugated rat anti-mouse κ-light chain (187.1, BD Biosciences) in a 0.1M Sodium carbonate-bicarbonate buffer (pH: 9.5). The next day, plates were blocked with 2% Bovine Serum Albumin (Millipore Sigma) in 1xPBS containing 0.05% Tween-20 (1xPBS-T) followed by incubation with serial dilutions of cell-free culture supernatants. After 3 hours, plates were then washed thrice with 1xPBS-T followed by an overnight incubation at $4^{O}C$ with biotinylated rat anti-mouse IgG2b (SB74g, Southern Biotech). Plates were washed the next day in 1xPBS-T followed by an incubation with Streptavidin linked to horseradish peroxidase (BD

Biosciences) for an hour at room temperature. Plates were developed using a TMB substrate (Alfa Aesar) and arrested with 2N Sulfuric acid (Millipore Sigma). Absorbance was measured at 450nm and corrected for background absorbance at 650nm on a VERSAmax microplate reader (Molecular devices). Area under the curve (AUC) was calculated from background adjusted A450 values on the Prism v.10.3 (Graphpad). A similar workflow was used for detection of NP-specific antibodies in serum, except that ELISA plates were coated with NP_{10-19}-BSA (Biosearch technologies) and detected with a Peroxidase-conjugated donkey anti-mouse IgG(H+L) (Jackson ImmunoResearch).

ELISpot

Multiscreen HTS HA filter plates (Millipore Sigma) were coated with NP-BSA (Biosearch technologies), Goat anti-mouse Ig(H+L) (Southern Biotech), or a 1:1 mix of Goat anti-human Lambda and Kappa (both from Southern Biotech) prepared in 1xPBS. After an overnight incubation at 4°C, plates were blocked with RPMI containing 10% FBS at 37°C. Sorted cells were resuspended in cRPMI and seeded in triplicates in their designated wells in the plate and incubated at 37°C overnight. Plates were washed the next day with 1xPBS and then incubated overnight with the following peroxidase-conjugated secondary reagents as appropriate: donkey anti-mouse IgG(H+L) for NP-specific plasma cells (Jackson Immunoresearch); goat anti-mouse IgM (1020-05), anti-IgG (1030-05), and anti-IgA (1040-05) for mouse splenic and bone marrow plasma cells; goat anti-human IgM (2020-05), anti-IgG (2045-05), and anti-IgA (2050-05) for detection of human bone marrow plasma cells (all from Southern Biotech). Spots were developed using a TrueBlue Peroxidase substrate (Kirkegaard and Perry Laboratories) and washed vigorously with MilliQ water. Spot size and numbers were quantified on the

CTL ImmunoSpot S6 analyzer. The total numbers of NP+ plasma cells were calculated by multiplying the number of spots with the dilution factor and divided by total bone marrow cell counts.

Statistical analysis

All statistical analysis was done using Prism v. 10.3 (Graphpad). Specific statistical tests and significance are indicated in the figure legends of the indicated graphs. Fold changes and p-values for the genome-wide screen were calculated by MaGeCK (*30*). Figure 2A was generated using Biorender.

Supplementary Materials

Figs. S1 to S6

References and Notes

1. W. E. Purtha, T. F. Tedder, S. Johnson, D. Bhattacharya, M. S. Diamond, Memory B cells, but not long-lived plasma cells, possess antigen specificities for viral escape mutants. *J Exp Med* **208**, 2599–2606 (2011).

2. I. J. Amanna, N. E. Carlson, M. K. Slifka, Duration of humoral immunity to common viral and vaccine antigens. *N Engl J Med* **357**, 1903–1915 (2007).

3. S.-E. Olsson, L. L. Villa, R. L. R. Costa, C. A. Petta, R. P. Andrade, C. Malm, O.-E. Iversen, J. Høye, M. Steinwall, G. Riis-Johannessen, A. Andersson-Ellstrom, K. Elfgren, G. von Krogh, M. Lehtinen, J. Paavonen, G. M. Tamms, K. Giacoletti, L. Lupinacci, M. T. Esser, S. C. Vuocolo, A. J. Saah, E. Barr, Induction of immune memory following administration of a prophylactic quadrivalent human papillomavirus (HPV) types 6/11/16/18 L1 virus-like particle (VLP) vaccine. *Vaccine* **25**, 4931–4939 (2007).

4. A. Olotu, G. Fegan, J. Wambua, G. Nyangweso, K. O. Awuondo, A. Leach, M. Lievens, D. Leboulleux, P. Njuguna, N. Peshu, K. Marsh, P. Bejon, Four-year efficacy of RTS,S/AS01E and its interaction with malaria exposure. *N Engl J Med* **368**, 1111–1120 (2013).

5. M. T. White, R. Verity, J. T. Griffin, K. P. Asante, S. Owusu-Agyei, B. Greenwood, C. Drakeley, S. Gesase, J. Lusingu, D. Ansong, S. Adjei, T. Agbenyega, B. Ogutu, L. Otieno, W. Otieno, S. T. Agnandji, B. Lell, P. Kremsner, I. Hoffman, F. Martinson, P. Kamthunzu, H. Tinto, I. Valea, H. Sorgho, M. Oneko, K. Otieno, M. J. Hamel, N. Salim, A. Mtoro, S. Abdulla, P. Aide, J. Sacarlal, J. J. Aponte, P.

Njuguna, K. Marsh, P. Bejon, E. M. Riley, A. C. Ghani, Immunogenicity of the RTS,S/AS01 malaria vaccine and implications for duration of vaccine efficacy: secondary analysis of data from a phase 3 randomised controlled trial. *Lancet Infect Dis* **15**, 1450–1458 (2015).

6. H. E. Mei, I. Wirries, D. Frölich, M. Brisslert, C. Giesecke, J. R. Grün, T. Alexander, S. Schmidt, K. Luda, A. A. Kühl, R. Engelmann, M. Dürr, T. Scheel, M. Bokarewa, C. Perka, A. Radbruch, T. Dörner, A unique population of IgG-expressing plasma cells lacking CD19 is enriched in human bone marrow. *Blood* **125**, 1739–1748 (2015).

7. J. L. Halliley, C. M. Tipton, J. Liesveld, A. F. Rosenberg, J. Darce, I. V. Gregoretti, L. Popova, D. Kaminiski, C. F. Fucile, I. Albizua, S. Kyu, K.-Y. Chiang, K. T. Bradley, R. Burack, M. Slifka, E. Hammarlund, H. Wu, L. Zhao, E. E. Walsh, A. R. Falsey, T. D. Randall, W. C. Cheung, I. Sanz, F. E.-H. Lee, Long-Lived Plasma Cells Are Contained within the CD19(-)CD38(hi)CD138(+) Subset in Human Bone Marrow. *Immunity* **43**, 132–145 (2015).

8. S. F. Brynjolfsson, M. Mohaddes, J. Kärrholm, M.-J. Wick, Long-lived plasma cells in human bone marrow can be either CD19+ or CD19. *Blood Adv* **1**, 835–838 (2017).

9. D. C. Nguyen, I. T. Hentenaar, A. Morrison-Porter, D. Solano, N. S. Haddad, C. Castrillon, M. C. Runnstrom, P. A. Lamothe, J. Andrews, D. Roberts, S. Lonial, I. Sanz, F. E.-H. Lee, SARS-CoV-2-specific plasma cells are not durably established

in the bone marrow long-lived compartment after mRNA vaccination. *Nat Med*, doi: 10.1038/s41591-024-03278-y (2024).

10. L. D'Souza, D. Bhattacharya, Plasma cells: You are what you eat. *Immunological Reviews* **288**, 161–177 (2019).

11. M. J. Robinson, Z. Ding, M. R. Dowling, D. L. Hill, R. H. Webster, C. McKenzie, C. Pitt, K. O'Donnell, J. Mulder, E. Brodie, P. D. Hodgkin, N. C. Wong, I. Quast, D. M. Tarlinton, Intrinsically determined turnover underlies broad heterogeneity in plasma-cell lifespan. *Immunity* **56**, 1596-1612.e4 (2023).

12. W. Y. Lam, A. Jash, C.-H. Yao, L. D'Souza, R. Wong, R. M. Nunley, G. P. Meares, G. J. Patti, D. Bhattacharya, Metabolic and Transcriptional Modules Independently Diversify Plasma Cell Lifespan and Function. *Cell Rep* **24**, 2479-2492.e6 (2018).

13. L. J. D'Souza, S. H. Wright, D. Bhattacharya, Genetic evidence that uptake of the fluorescent analog 2NBDG occurs independently of known glucose transporters. *PLoS One* **17**, e0261801 (2022).

14. O. Yanagida, Y. Kanai, A. Chairoungdua, D. K. Kim, H. Segawa, T. Nii, S. H. Cha, H. Matsuo, J. Fukushima, Y. Fukasawa, Y. Tani, Y. Taketani, H. Uchino, J. Y. Kim, J. Inatomi, I. Okayasu, K. Miyamoto, E. Takeda, T. Goya, H. Endou, Human L-type amino acid transporter 1 (LAT1): characterization of function and expression in tumor cell lines. *Biochim Biophys Acta* **1514**, 291–302 (2001).

15. J. M. Cantor, M. H. Ginsberg, CD98 at the crossroads of adaptive immunity and cancer. *J Cell Sci* **125**, 1373–1382 (2012).

16. C. C. Feral, N. Nishiya, C. A. Fenczik, H. Stuhlmann, M. Slepak, M. H. Ginsberg, CD98hc (SLC3A2) mediates integrin signaling. *Proc Natl Acad Sci U S A* **102**, 355–360 (2005).

17. J. Tellier, W. Shi, M. Minnich, Y. Liao, S. Crawford, G. K. Smyth, A. Kallies, M. Busslinger, S. L. Nutt, Blimp-1 controls plasma cell function through the regulation of immunoglobulin secretion and the unfolded protein response. *Nat Immunol* **17**, 323–330 (2016).

18. M. Minnich, H. Tagoh, P. Bönelt, E. Axelsson, M. Fischer, B. Cebolla, A. Tarakhovsky, S. L. Nutt, M. Jaritz, M. Busslinger, Multifunctional role of the transcription factor Blimp-1 in coordinating plasma cell differentiation. *Nat Immunol* **17**, 331–343 (2016).

19. K. Martincic, S. A. Alkan, A. Cheatle, L. Borghesi, C. Milcarek, Transcription elongation factor ELL2 directs immunoglobulin secretion in plasma cells by stimulating altered RNA processing. *Nat Immunol* **10**, 1102–1109 (2009).

20. A. M. Reimold, N. N. Iwakoshi, J. Manis, P. Vallabhajosyula, E. Szomolanyi-Tsuda, E. M. Gravallese, D. Friend, M. J. Grusby, F. Alt, L. H. Glimcher, Plasma cell differentiation requires the transcription factor XBP-1. *Nature* **412**, 300–307 (2001).

21. A. L. Shaffer, M. Shapiro-Shelef, N. N. Iwakoshi, A.-H. Lee, S.-B. Qian, H. Zhao, X. Yu, L. Yang, B. K. Tan, A. Rosenwald, E. M. Hurt, E. Petroulakis, N. Sonenberg, J. W. Yewdell, K. Calame, L. H. Glimcher, L. M. Staudt, XBP1, downstream of Blimp-

1, expands the secretory apparatus and other organelles, and increases protein synthesis in plasma cell differentiation. *Immunity* **21**, 81–93 (2004).

22. C.-C. A. Hu, S. K. Dougan, S. V. Winter, A. W. Paton, J. C. Paton, H. L. Ploegh, Subtilase cytotoxin cleaves newly synthesized BiP and blocks antibody secretion in B lymphocytes. *J Exp Med* **206**, 2429–2440 (2009).

23. N. Taubenheim, D. M. Tarlinton, S. Crawford, L. M. Corcoran, P. D. Hodgkin, S. L. Nutt, High rate of antibody secretion is not integral to plasma cell differentiation as revealed by XBP-1 deficiency. *J Immunol* **189**, 3328–3338 (2012).

24. D. D. Jones, B. T. Gaudette, J. R. Wilmore, I. Chernova, A. Bortnick, B. M. Weiss, D. Allman, mTOR has distinct functions in generating versus sustaining humoral immunity. *J Clin Invest* **126**, 4250–4261 (2016).

25. S. Benhamron, S. P. Pattanayak, M. Berger, B. Tirosh, mTOR activation promotes plasma cell differentiation and bypasses XBP-1 for immunoglobulin secretion. *Mol Cell Biol* **35**, 153–166 (2015).

26. S. K. Brookens, S. H. Cho, P. J. Basso, M. R. Boothby, AMPKα1 in B Cells Dampens Primary Antibody Responses yet Promotes Mitochondrial Homeostasis and Persistence of B Cell Memory. *J Immunol* **205**, 3011–3022 (2020).

27. J. R. Wilmore, B. T. Gaudette, D. Gomez Atria, T. Hashemi, D. D. Jones, C. A. Gardner, S. D. Cole, A. M. Misic, D. P. Beiting, D. Allman, Commensal Microbes Induce Serum IgA Responses that Protect against Polymicrobial Sepsis. *Cell Host Microbe* **23**, 302-311.e3 (2018).

28. W. Shi, Y. Liao, S. N. Willis, N. Taubenheim, M. Inouye, D. M. Tarlinton, G. K. Smyth, P. D. Hodgkin, S. L. Nutt, L. M. Corcoran, Transcriptional profiling of mouse B cell terminal differentiation defines a signature for antibody-secreting plasma cells. *Nat Immunol* **16**, 663–673 (2015).

29. J. G. Doench, N. Fusi, M. Sullender, M. Hegde, E. W. Vaimberg, K. F. Donovan, I. Smith, Z. Tothova, C. Wilen, R. Orchard, H. W. Virgin, J. Listgarten, D. E. Root, Optimized sgRNA design to maximize activity and minimize off-target effects of CRISPR-Cas9. *Nat Biotechnol* **34**, 184–191 (2016).

30. W. Li, H. Xu, T. Xiao, L. Cong, M. I. Love, F. Zhang, R. A. Irizarry, J. S. Liu, M. Brown, X. S. Liu, MAGeCK enables robust identification of essential genes from genome-scale CRISPR/Cas9 knockout screens. *Genome Biol* **15**, 554 (2014).

31. M. P. Collins, M. Forgac, Regulation and function of V-ATPases in physiology and disease. *Biochim Biophys Acta Biomembr* **1862**, 183341 (2020).

32. J. R. Casey, S. Grinstein, J. Orlowski, Sensors and regulators of intracellular pH. *Nat Rev Mol Cell Biol* **11**, 50–61 (2010).

33. E. J. Bowman, A. Siebers, K. Altendorf, Bafilomycins: a class of inhibitors of membrane ATPases from microorganisms, animal cells, and plant cells. *Proc Natl Acad Sci U S A* **85**, 7972–7976 (1988).

34. B. A. Webb, F. M. Aloisio, R. A. Charafeddine, J. Cook, T. Wittmann, D. L. Barber, pHLARE: a new biosensor reveals decreased lysosome pH in cancer cells. *Mol Biol Cell* **32**, 131–142 (2021).

35. J.-D. Pédelacq, S. Cabantous, T. Tran, T. C. Terwilliger, G. S. Waldo, Engineering and characterization of a superfolder green fluorescent protein. *Nat Biotechnol* **24**, 79–88 (2006).

36. R. Meyers, L. C. Cantley, Cloning and characterization of a wortmannin-sensitive human phosphatidylinositol 4-kinase. *J Biol Chem* **272**, 4384–4390 (1997).

37. A. Godi, P. Pertile, R. Meyers, P. Marra, G. Di Tullio, C. Iurisci, A. Luini, D. Corda, M. A. De Matteis, ARF mediates recruitment of PtdIns-4-OH kinase-beta and stimulates synthesis of PtdIns(4,5)P2 on the Golgi complex. *Nat Cell Biol* **1**, 280–287 (1999).

38. T. Baba, T. Balla, Emerging roles of phosphatidylinositol 4-phosphate and phosphatidylinositol 4,5-bisphosphate as regulators of multiple steps in autophagy. *J Biochem* **168**, 329–336 (2020).

39. M.-C. Lai, Y.-H. W. Lee, W.-Y. Tarn, The DEAD-box RNA helicase DDX3 associates with export messenger ribonucleoproteins as well as tip-associated protein and participates in translational control. *Mol Biol Cell* **19**, 3847–3858 (2008).

40. R. Soto-Rifo, P. S. Rubilar, T. Limousin, S. de Breyne, D. Décimo, T. Ohlmann, DEAD-box protein DDX3 associates with eIF4F to promote translation of selected mRNAs. *EMBO J* **31**, 3745–3756 (2012).

41. L. Calviello, S. Venkataramanan, K. J. Rogowski, E. Wyler, K. Wilkins, M. Tejura, B. Thai, J. Krol, W. Filipowicz, M. Landthaler, S. N. Floor, DDX3 depletion

722 represses translation of mRNAs with complex 5’ UTRs. *Nucleic Acids Res* **49**,
723 5336–5350 (2021).

724 42. A. L. Lennox, M. L. Hoye, R. Jiang, B. L. Johnson-Kerner, L. A. Suit, S.
725 Venkataramanan, C. J. Sheehan, F. C. Alsina, B. Fregeau, K. A. Aldinger, C.
726 Moey, I. Lobach, A. Afenjar, D. Babovic-Vuksanovic, S. Bézieau, P. R. Blackburn,
727 J. Bunt, L. Burglen, P. M. Campeau, P. Charles, B. H. Y. Chung, B. Cogné, C.
728 Curry, M. D. D’Agostino, N. Di Donato, L. Faivre, D. Héron, A. M. Innes, B. Isidor,
729 B. Keren, A. Kimball, E. W. Klee, P. Kuentz, S. Küry, D. Martin-Coignard, G.
730 Mirzaa, C. Mignot, N. Miyake, N. Matsumoto, A. Fujita, C. Nava, M. Nizon, D.
731 Rodriguez, L. S. Blok, C. Thauvin-Robinet, J. Thevenon, M. Vincent, A. Ziegler, W.
732 Dobyns, L. J. Richards, A. J. Barkovich, S. N. Floor, D. L. Silver, E. H. Sherr,
733 Pathogenic DDX3X Mutations Impair RNA Metabolism and Neurogenesis during
734 Fetal Cortical Development. *Neuron* **106**, 404-420.e8 (2020).

735 43. K. Takeda, S. Akira, TLR signaling pathways. *Semin Immunol* **16**, 3–9 (2004).

736 44. C. Pasare, R. Medzhitov, Control of B-cell responses by Toll-like receptors. *Nature*
737 **438**, 364–368 (2005).

738 45. B. He, R. Santamaria, W. Xu, M. Cols, K. Chen, I. Puga, M. Shan, H. Xiong, J. B.
739 Bussel, A. Chiu, A. Puel, J. Reichenbach, L. Marodi, R. Döffinger, J. Vasconcelos,
740 A. Issekutz, J. Krause, G. Davies, X. Li, B. Grimbacher, A. Plebani, E. Meffre, C.
741 Picard, C. Cunningham-Rundles, J.-L. Casanova, A. Cerutti, The transmembrane
742 activator TACI triggers immunoglobulin class switching by activating B cells
743 through the adaptor MyD88. *Nat Immunol* **11**, 836–845 (2010).

46. B. Hou, B. Reizis, A. L. DeFranco, Toll-like receptors activate innate and adaptive immunity by using dendritic cell-intrinsic and -extrinsic mechanisms. *Immunity* **29**, 272–282 (2008).

47. R. Wong, J. A. Belk, J. Govero, J. L. Uhrlaub, D. Reinartz, H. Zhao, J. M. Errico, L. D'Souza, T. J. Ripperger, J. Nikolich-Zugich, M. J. Shlomchik, A. T. Satpathy, D. H. Fremont, M. S. Diamond, D. Bhattacharya, Affinity-Restricted Memory B Cells Dominate Recall Responses to Heterologous Flaviviruses. *Immunity* **53**, 1078-1094.e7 (2020).

48. A. L. Gavin, K. Hoebe, B. Duong, T. Ota, C. Martin, B. Beutler, D. Nemazee, Adjuvant-enhanced antibody responses in the absence of toll-like receptor signaling. *Science* **314**, 1936–1938 (2006).

49. E. J. Pone, T. Lam, Z. Lou, R. Wang, Y. Chen, D. Liu, A. L. Edinger, Z. Xu, P. Casali, B cell Rab7 mediates induction of activation-induced cytidine deaminase expression and class-switching in T-dependent and T-independent antibody responses. *J Immunol* **194**, 3065–3078 (2015).

50. T. Lam, D. V. Kulp, R. Wang, Z. Lou, J. Taylor, C. E. Rivera, H. Yan, Q. Zhang, Z. Wang, H. Zan, D. N. Ivanov, G. Zhong, P. Casali, Z. Xu, Small Molecule Inhibition of Rab7 Impairs B Cell Class Switching and Plasma Cell Survival To Dampen the Autoantibody Response in Murine Lupus. *J Immunol* **197**, 3792–3805 (2016).

51. A. Balla, G. Tuymetova, M. Barshishat, M. Geiszt, T. Balla, Characterization of type II phosphatidylinositol 4-kinase isoforms reveals association of the enzymes with endosomal vesicular compartments. *J Biol Chem* **277**, 20041–20050 (2002).

52. S. Sridhar, B. Patel, D. Aphkhazava, F. Macian, L. Santambrogio, D. Shields, A. M. Cuervo, The lipid kinase PI4KIIIβ preserves lysosomal identity. *EMBO J* **32**, 324–339 (2013).

53. J.-W. Shih, T.-Y. Tsai, C.-H. Chao, Y.-H. Wu Lee, Candidate tumor suppressor DDX3 RNA helicase specifically represses cap-dependent translation by acting as an eIF4E inhibitory protein. *Oncogene* **27**, 700–714 (2008).

54. D. Szappanos, R. Tschismarov, T. Perlot, S. Westermayer, K. Fischer, E. Platanitis, F. Kallinger, M. Novatchkova, C. Lassnig, M. Müller, V. Sexl, K. L. Bennett, M. Foong-Sobis, J. M. Penninger, T. Decker, The RNA helicase DDX3X is an essential mediator of innate antimicrobial immunity. *PLoS Pathog* **14**, e1007397 (2018).

55. K. Liu, J. Tuazon, E. P. Karmele, D. Krishnamurthy, T. Perlor, M. Foong-Sobis, R. A. Karns, M. Mandal, D. Reynaud, R. H. Scofield, J. M. Penninger, J. B. Harley, S. N. Waggoner, *Ddx3x* regulates B-cell development and light chain recombination in mice. [Preprint] (2018). https://doi.org/10.1101/452086.

56. T. Sekiguchi, H. Iida, J. Fukumura, T. Nishimoto, Human DDX3Y, the Y-encoded isoform of RNA helicase DDX3, rescues a hamster temperature-sensitive ET24 mutant cell line with a DDX3X mutation. *Exp Cell Res* **300**, 213–222 (2004).

57. M. J. Benson, S. R. Dillon, E. Castigli, R. S. Geha, S. Xu, K.-P. Lam, R. J. Noelle, Cutting edge: the dependence of plasma cells and independence of memory B cells on BAFF and APRIL. *J Immunol* **180**, 3655–3659 (2008).

58. M. Eslami, S. Schuepbach-Mallepell, D. Diana, L. Willen, C. Kowalczyk-Quintas, C. Desponds, B. Peter, M. Vigolo, F. Renevey, O. Donzé, S. A. Luther, Ö. Yalkinoglu, N. Alouche, P. Schneider, Unique and redundant roles of mouse BCMA, TACI, BAFF, APRIL, and IL-6 in supporting antibody-producing cells in different tissues. *Proc Natl Acad Sci U S A* **121**, e2404309121 (2024).

59. G. Cassese, S. Arce, A. E. Hauser, K. Lehnert, B. Moewes, M. Mostarac, G. Muehlinghaus, M. Szyska, A. Radbruch, R. A. Manz, Plasma cell survival is mediated by synergistic effects of cytokines and adhesion-dependent signals. *J Immunol* **171**, 1684–1690 (2003).

60. E. Belnoue, M. Pihlgren, T. L. McGaha, C. Tougne, A.-F. Rochat, C. Bossen, P. Schneider, B. Huard, P.-H. Lambert, C.-A. Siegrist, APRIL is critical for plasmablast survival in the bone marrow and poorly expressed by early-life bone marrow stromal cells. *Blood* **111**, 2755–2764 (2008).

61. H.-Y. Huang, A. Rivas-Caicedo, F. Renevey, H. Cannelle, E. Peranzoni, L. Scarpellino, D. L. Hardie, A. Pommier, K. Schaeuble, S. Favre, T. K. Vogt, F. Arenzana-Seisdedos, P. Schneider, C. D. Buckley, E. Donnadieu, S. A. Luther, Identification of a new subset of lymph node stromal cells involved in regulating plasma cell homeostasis. *Proc Natl Acad Sci U S A* **115**, E6826–E6835 (2018).

62. D. C. Nguyen, S. Garimalla, H. Xiao, S. Kyu, I. Albizua, J. Galipeau, K.-Y. Chiang, E. K. Waller, R. Wu, G. Gibson, J. Roberson, F. E. Lund, T. D. Randall, I. Sanz, F. E.-H. Lee, Factors of the bone marrow microniche that support human plasma cell survival and immunoglobulin secretion. *Nat Commun* **9**, 3698 (2018).

63. L. Yu, L. Wang, S. Chen, Endogenous toll-like receptor ligands and their biological significance. *J Cell Mol Med* **14**, 2592–2603 (2010).

64. T. Pinter, M. Fischer, M. Schäfer, M. Fellner, J. Jude, J. Zuber, M. Busslinger, M. Wöhner, Comprehensive CRISPR-Cas9 screen identifies factors which are important for plasmablast development. *Front Immunol* **13**, 979606 (2022).

65. E. Xiong, O. Popp, C. Salomon, P. Mertins, C. Kocks, K. Rajewsky, V. T. Chu, A CRISPR/Cas9-mediated screen identifies determinants of early plasma cell differentiation. *Front Immunol* **13**, 1083119 (2022).

66. S. Trezise, I. Y. Kong, E. D. Hawkins, M. J. Herold, S. N. Willis, S. L. Nutt, An arrayed CRISPR screen of primary B cells reveals the essential elements of the antibody secretion pathway. *Front Immunol* **14**, 1089243 (2023).

67. N. E. Sanjana, O. Shalem, F. Zhang, Improved vectors and genome-wide libraries for CRISPR screening. *Nat Methods* **11**, 783–784 (2014).

68. P. K.-S. Ng, J. Li, K. J. Jeong, S. Shao, H. Chen, Y. H. Tsang, S. Sengupta, Z. Wang, V. H. Bhavana, R. Tran, S. Soewito, D. C. Minussi, D. Moreno, K. Kong, T. Dogruluk, H. Lu, J. Gao, C. Tokheim, D. C. Zhou, A. M. Johnson, J. Zeng, C. K. M. Ip, Z. Ju, M. Wester, S. Yu, Y. Li, C. P. Vellano, N. Schultz, R. Karchin, L. Ding, Y.

Lu, L. W. T. Cheung, K. Chen, K. R. Shaw, F. Meric-Bernstam, K. L. Scott, S. Yi, N. Sahni, H. Liang, G. B. Mills, Systematic Functional Annotation of Somatic Mutations in Cancer. *Cancer Cell* **33**, 450-462.e10 (2018).

69. K. R. Sanson, R. E. Hanna, M. Hegde, K. F. Donovan, C. Strand, M. E. Sullender, E. W. Vaimberg, A. Goodale, D. E. Root, F. Piccioni, J. G. Doench, Optimized libraries for CRISPR-Cas9 genetic screens with multiple modalities. *Nat Commun* **9**, 5416 (2018).

70. I. R. Garrett, S. Dallas, J. Radl, G. R. Mundy, A murine model of human myeloma bone disease. *Bone* **20**, 515–520 (1997).

Acknowledgments: The authors wish to thank the flow cytometry core at the University of Arizona for their assistance. We are also grateful to Colin Fields for his assistance in procuring human samples after surgery and Jean Wilson, Hannah Pizzato, and Kit Tobey for their inputs. We also wish to thank William Smith and the staff at University Animal Care for their assistance with mouse husbandry and maintenance.

Funding: The funders of this project had no role in study design, data collection and interpretation, decision to publish, or composing the manuscript. There was no additional external funding received for this study.

National Institutes of Health grant R01AI129945 (DB)

National Cancer Institute grant P30CA023074

National Institutes of Health grant S10OD028466 (DB)

Bio5 postdoctoral fellowship (LJD)

Author contributions:

Conceptualization: DB and LJD

Methodology: DB and LJD

Investigation: LJD, JNY, HC, EPP, and DB

Visualization: DB and LJD

Funding acquisition: DB

Project administration: DB

Supervision: DB

Writing – original draft: LJD, JNY, HC, EPP, and DB

Writing – review & editing: LJD, JNY, HC, EPP, and DB

Competing interests: Sana Biotechnology has licensed intellectual property of DB and Washington University in St. Louis. Inograft biotherapeutics and Jasper Therapeutics have licensed intellectual property of DB and Stanford University. D.B. is on the scientific advisory board for Hillevax. LJD, JNY, HC, and EPP report no conflict of interest.

Data and materials availability: All data are available in the main text or the supplementary materials.

Figure 1

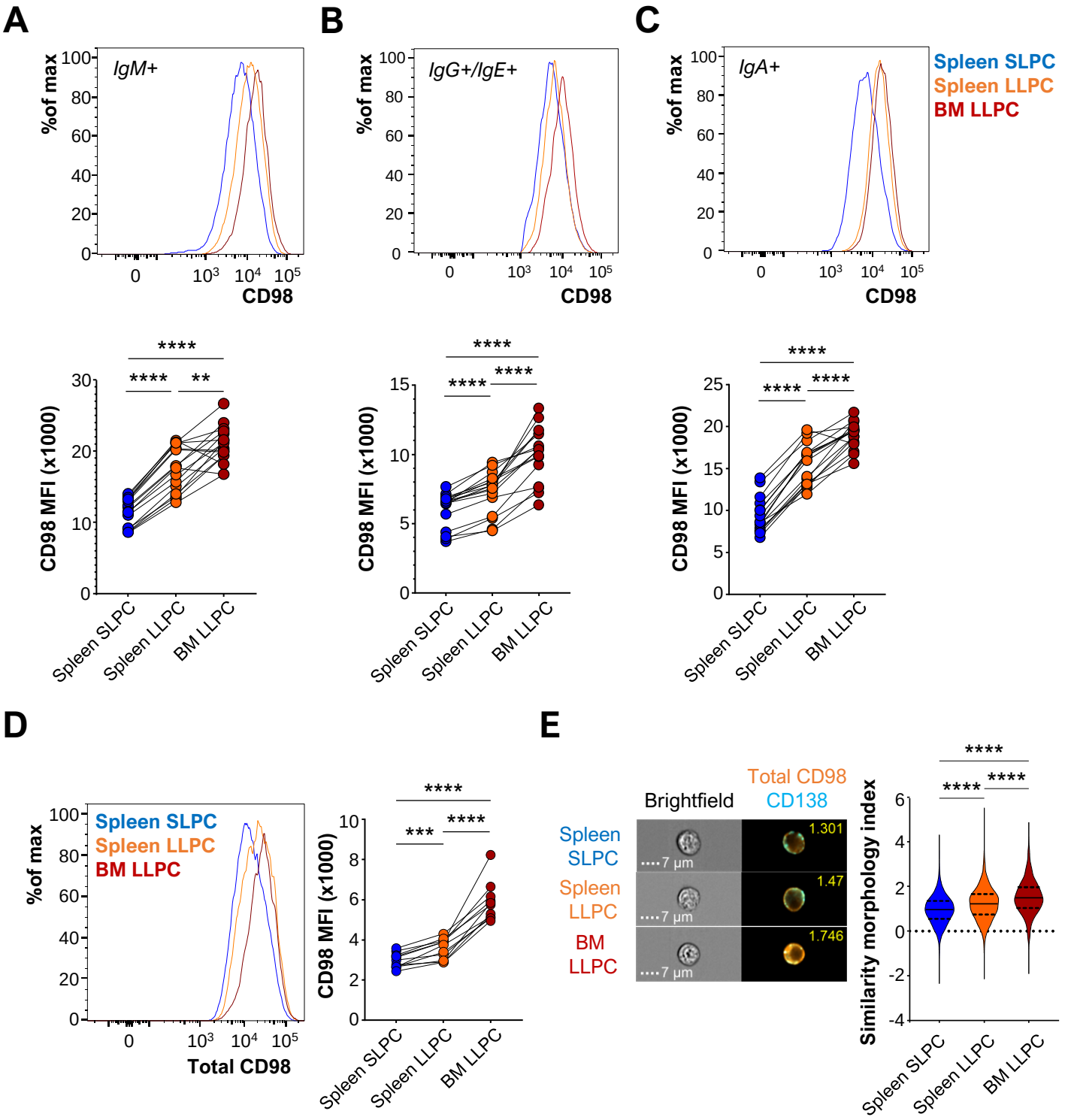
A
B
C
IgM+
IgG+/IgE+
IgA+
%of max
CD98
Spleen SLPC
Spleen LLPC
BM LLPC
CD98 MFI (x1000)
****
**
D
E
Total CD98
Brightfield
CD138
1.301
1.47
1.746
7 µm
***
Similarity morphology index

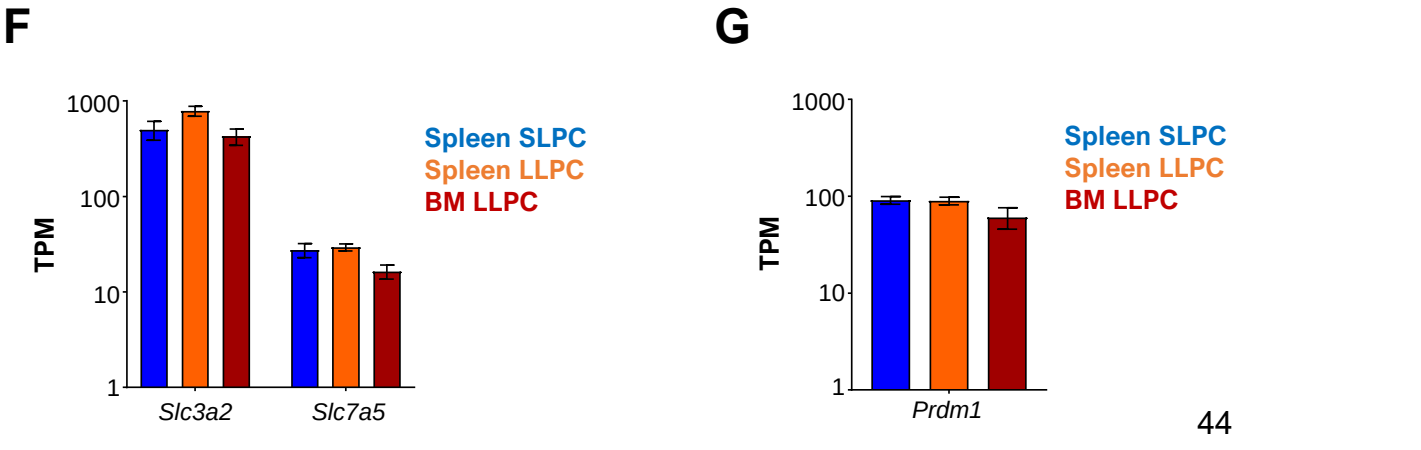
F
G
TPM
Slc3a2
Slc7a5
Prdm1
Spleen SLPC
Spleen LLPC
BM LLPC

Figure Legends

Fig. 1. LLPCs have higher levels of CD98 than SLPCs despite having similar transcript reads

(A-C) Representative histograms (top) and quantification of mean fluorescence intensity (MFI) values (bottom) of CD98 expression on *ex vivo* (A) IgM+, (B) IgG+ and IgE+, and (C) IgA+ plasma cell subsets. Each data point represents cells from one mouse, and subsets from each mouse are connected by lines. Pooled data from 16 mice across 4 experiments. *p<0.05 by Tukey's multiple comparisons test.

(D) Representative histogram of total (surface and internal) CD98 protein levels in sorted plasma cell subsets (left). Quantification of total CD98 MFI of each subset is represented (right). Each data point represents cells from one mouse, and subsets from each mouse are connected by lines. Pooled data from 11 mice across 3 experiments. *p<0.05 by Tukey's multiple comparisons test.

(E) Cells in (D) were examined by imaging flow cytometry. Representative images for each subset are shown with surface CD138 (cyan) and total CD98 (orange) and their colocalization. Similarity morphology indices are indicated on the top right of the image and values for each subset are quantified. Representative graph of one of three independent experiments. *P<0.05 by Games-Howell's multiple comparisons test.

(F) Transcripts per million kilobase (TPM) values of CD98hc (*Slc3a2*) and CD98lc (*Slc7a5*) from Lam WY *et al* (Cell Reports 2018), showing values across splenic and bone marrow plasma cell subsets. Pooled data from three independent experiments.

(G) Transcripts per million kilobase (TPM) values for BLIMP1 (*Prdm1*) from Lam WY *et al* (Cell Reports 2018) across splenic and bone marrow plasma cell subsets. Pooled data from three independent experiments.

Figure 2

A

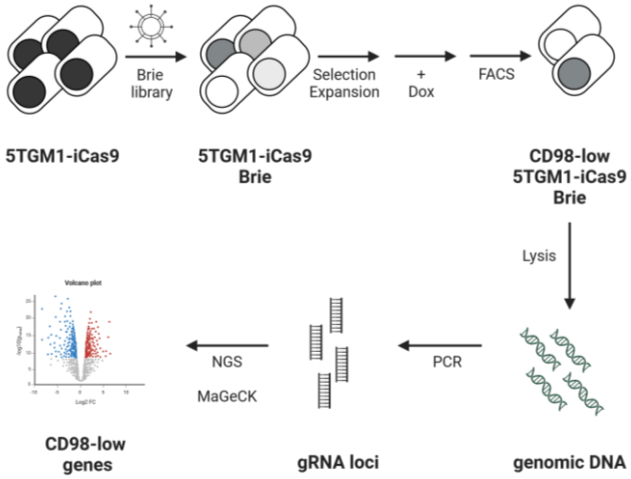

B

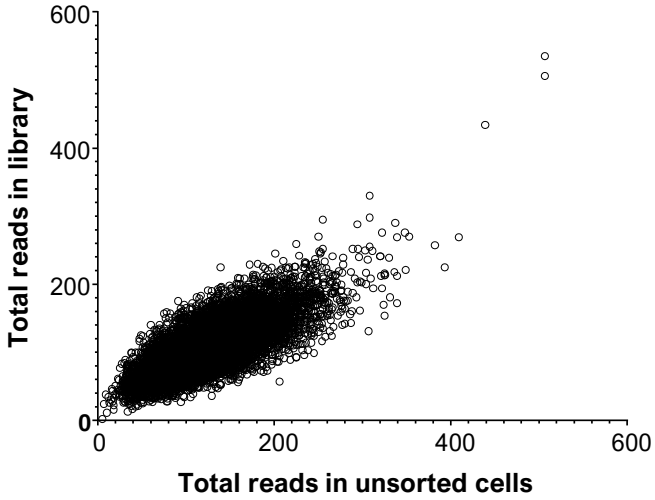

C

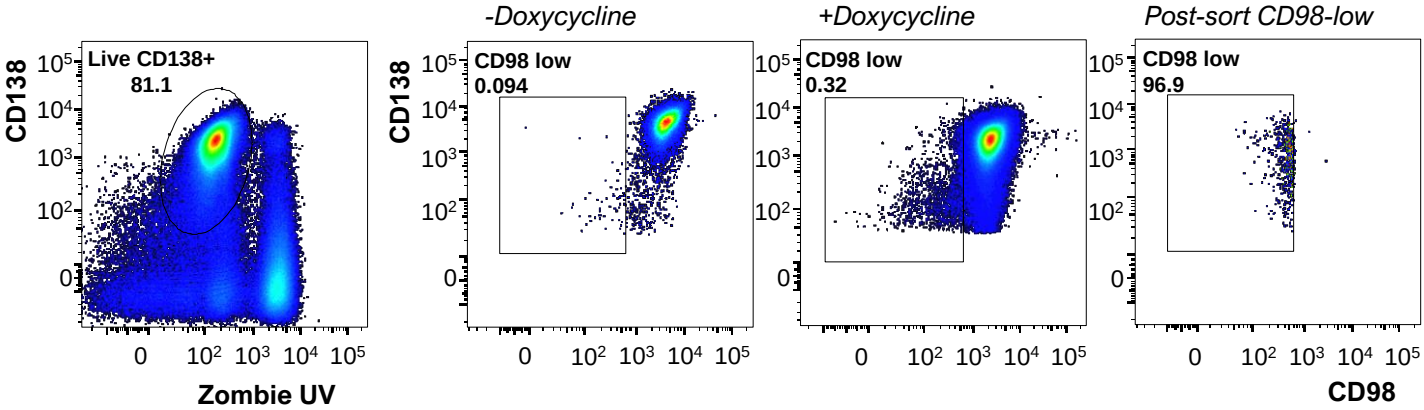

D

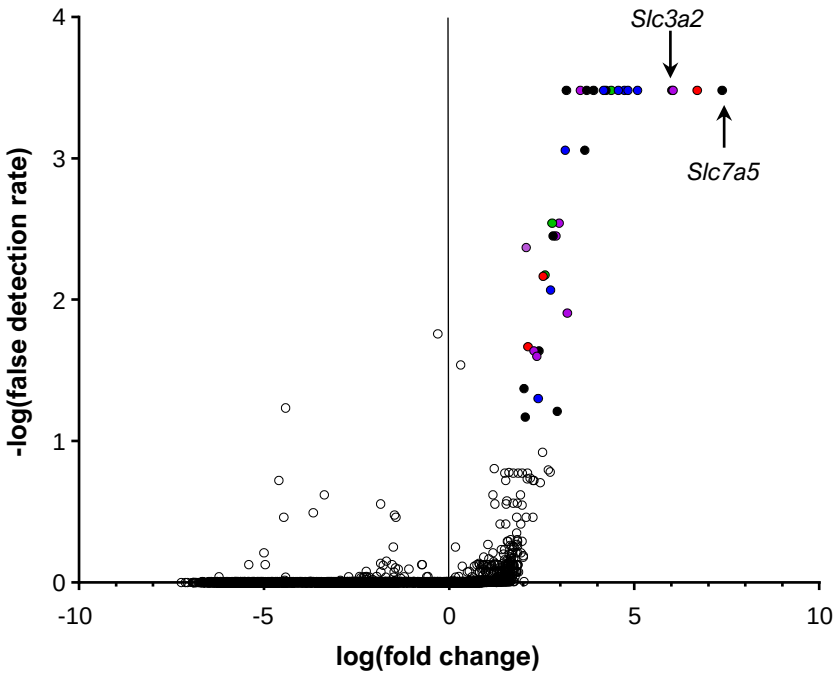

V-type ATPases
Atp6v0b
Atp6v0c
Atp6v0d1
Atp6v0e
Atp6v1a
Atp6v1b2
Atp6v1e1
Atp6v1g1

Vesicular proteins
Exoc5
Exoc8
Gosr2
Nsf
Scfd1
Stx4a
Trappc5
Trappc8

Signaling intermediates
Pi4kb
Myc
Myd88

RNA binding proteins
Ddx3x
Nob1
Rbm33
RnaseK

Fig. 2. Genes involved in vesicle biology and exocytosis promote plasma cell CD98 expression

(A) Schematic of genome-wide unbiased CRISPR-Cas9 screen in 5TGM1 cells.

(B) Scatter plot of gRNA read counts following next-generation sequencing of the mouse Brie library (Y axis) against the corresponding read numbers in uninduced 5TGM1-iCas9-Brie cells (X axis). Each open circle represents one gRNA.

(C) Representative gating on 5TGM1-iCas9 transduced with the mouse Brie gRNA library. After treatment with Doxycycline for 7 days, 5TGM1-iCas9-Brie cells were gated first to exclude dead cells and debris (far left). On this gate, cells were subsequently gated as CD98-low based on the untreated 5TGM1-iCas9-Brie cells (center left). CD98-low cells in Doxycycline treated cultures (center right) were then purified by FACS to achieve a pure CD98-low fraction (far right).

(D) MAGeCK analysis of genes enriched in the CD98-low fraction relative to unsorted 5TGM1-iCas9 cells transduced with the Brie library. Volcano plot of fold change between sorted cells against control cells are shown. Statistically significant genes are indicated as filled circles, the color of which corresponds to the class of genes indicated next to the volcano graph. Four biological replicates were analyzed.

Figure 3

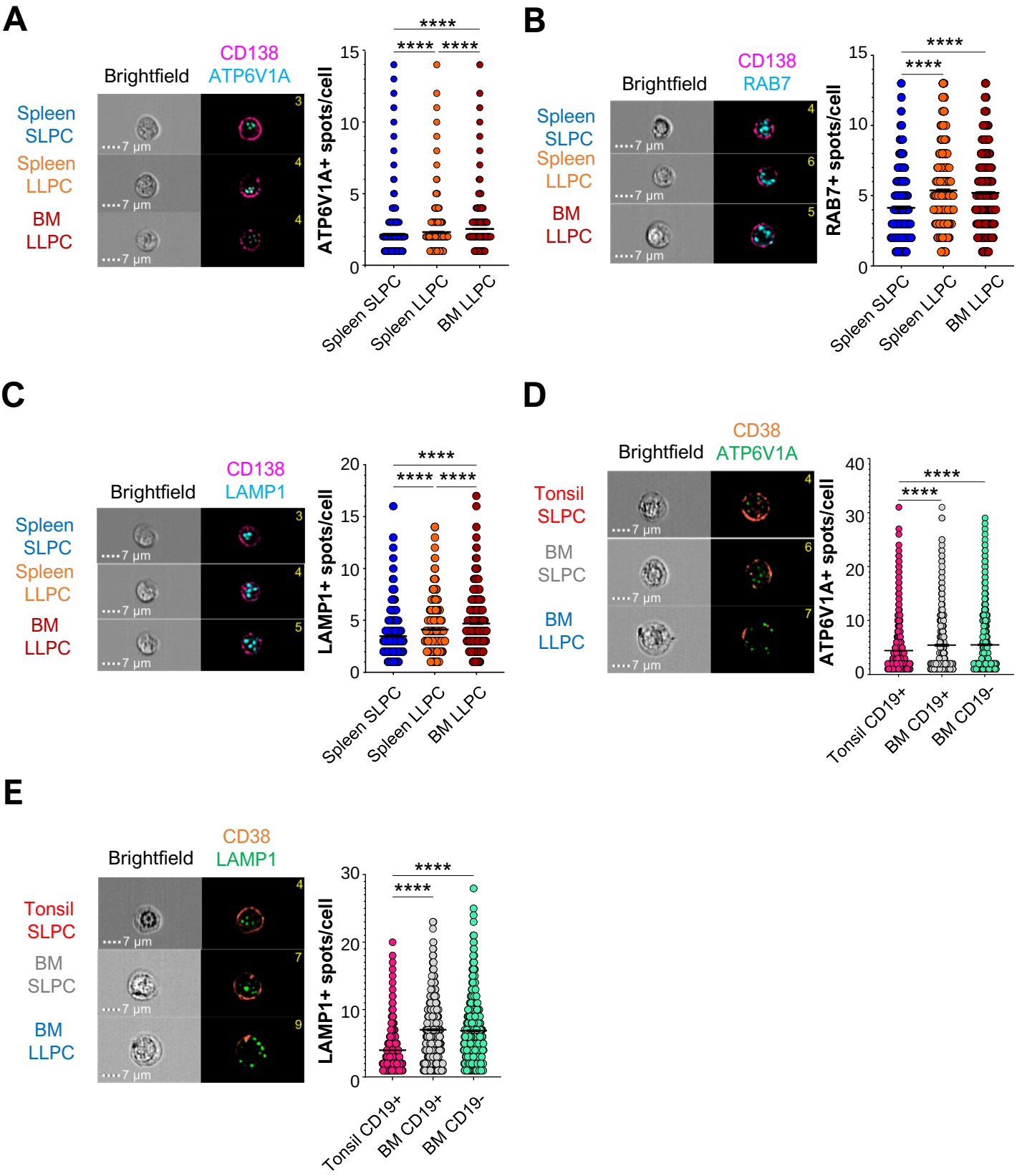
A
Brightfield
CD138
ATP6V1A
Spleen SLPC
Spleen LLPC
BM LLPC
7 µm
ATP6V1A+ spots/cell
Spleen SLPC
Spleen LLPC
BM LLPC
B
Brightfield
CD138
RAB7
RAB7+ spots/cell
C
Brightfield
CD138
LAMP1
LAMP1+ spots/cell
D
Brightfield
CD38
ATP6V1A
Tonsil SLPC
BM SLPC
BM LLPC
Tonsil CD19+
BM CD19+
BM CD19-
E
Brightfield
CD38
LAMP1
****

Fig. 3. LLPCs have higher frequencies of acidic vacuoles than SLPCs

(A) Mouse plasma cell subsets from the spleen and bone marrow were sorted and stained for surface CD138 (pink) and intracellular ATP6V1A protein (cyan) and cells analyzed by imaging flow cytometry. ATP6V1A spot numbers/cell were enumerated and mean +/- SEM shown. Combined data from 9890-10755 cells from 12 mice across 3 experiments. *p<0.05 by Games-Howell's multiple comparisons test.

(B) Mouse plasma cell subsets as in (A) were stained for surface CD138 (pink) and RAB7 (cyan). RAB7+ spot numbers/cell were enumerated and mean +/- SEM graphed. Pooled data from 1639-2115 cells from 12 mice across 3 experiments. *p<0.05 by Games-Howell's multiple comparisons test.

(C) Mouse plasma cell subsets as in (A) were stained for surface CD138 (pink) and LAMP1 (cyan). LAMP1+ spot numbers/cell were enumerated and mean +/- SEM graphed. Pooled data from 3061-9159 cells from 12 mice across 3 experiments. *p<0.05 by Games-Howell's multiple comparisons test.

(D) Human plasma cells from the tonsil (CD19+ CD38+ CD27+ CD138-) and bone marrow CD19+ and CD19- plasma cells (CD27+ CD38+ CD138+) were stained for surface CD38 (orange) and intracellular ATP6V1A protein. ATP6V1A+ spot numbers/cell were quantified and mean +/- SEM plotted for all subsets. Combined data from 1156-9050 cells from 7 tonsil donors and 6 bone marrow donors across 3 experiments. *p<0.05 by Games-Howell's multiple comparisons test.

(E) Human plasma cell subsets as in (D) were stained for surface CD38 and intracellular LAMP1. LAMP1+ spot numbers/cell were quantified and mean +/- SEM

plotted. Pooled data from 2614-10742 cells from 9 tonsil donors and 7 bone marrow donors from 4 experiments. *$p<0.05$ by Games-Howell's multiple comparisons test.

Figure 4

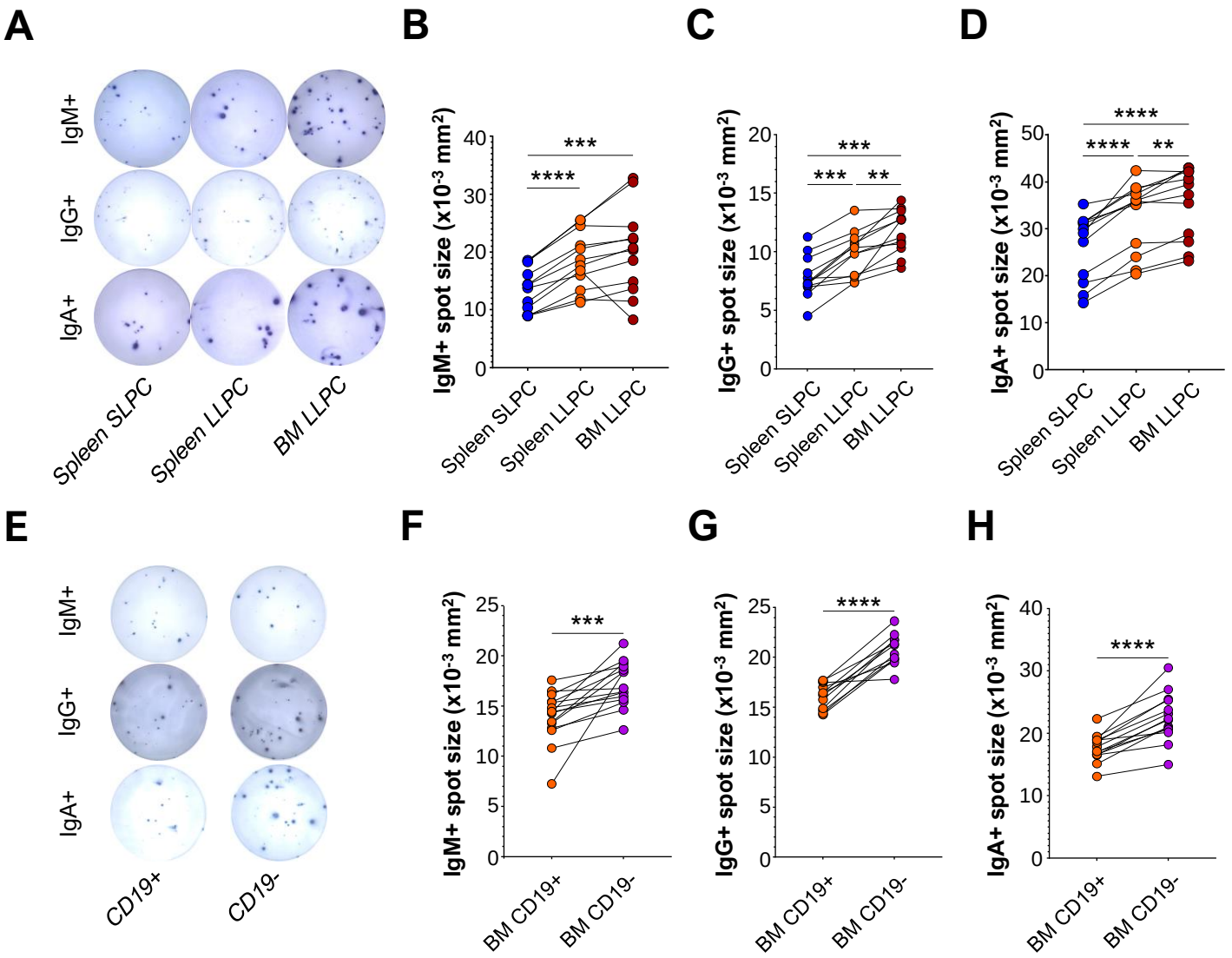
A
IgM+
IgG+
IgA+
Spleen SLPC
Spleen LLPC
BM LLPC
B
IgM+ spot size (x10-3 mm2)
***
****
C
IgG+ spot size (x10-3 mm2)
***
***
**
D
IgA+ spot size (x10-3 mm2)
****
****
**
E
IgM+
IgG+
IgA+
CD19+
CD19-
F
IgM+ spot size (x10-3 mm2)
***
BM CD19+
BM CD19-
G
IgG+ spot size (x10-3 mm2)
****
H
IgA+ spot size (x10-3 mm2)
****

Fig. 4. LLPCs secrete more antibodies than SLPCs independent of immunoglobulin isotype

(A-D) IgM+ *ex vivo* splenic SLPCs, LLPCs, and bone marrow LLPCs were sorted and seeded into wells of an ELISpot plate. (A) Representative images showing spots for each subset and isotype are indicated. Quantification of (B) IgM+, (C) IgG+, and (D) IgA+ plasma cell spot area of each subset is represented. Each data point represents mean spot sizes from one mouse, and subsets within each mouse are connected by lines. Pooled data from 12 mice across 3 experiments. *$p<0.05$ by Tukey's multiple comparisons test.

(E-H) Human bone marrow plasma cells (CD27+ CD38+ CD138+) were sorted as CD19+ and CD19- populations and seeded into wells of an ELISpot plate. (E) Representative images showing spots for CD19+/- plasma cells secreting the indicated isotype are shown. Quantification of spot area of (F) IgM+, (G) IgG+, and (H) IgA+ plasma cells are represented. Each data point represents one donor, and subsets from an individual are connected by lines. Pooled data from 15 donors across 4 experiments for IgM, 12 donors across 3 experiments for IgG, and 14 donors across 4 experiments for IgA. *$p<0.05$ by paired t test.

Figure 5

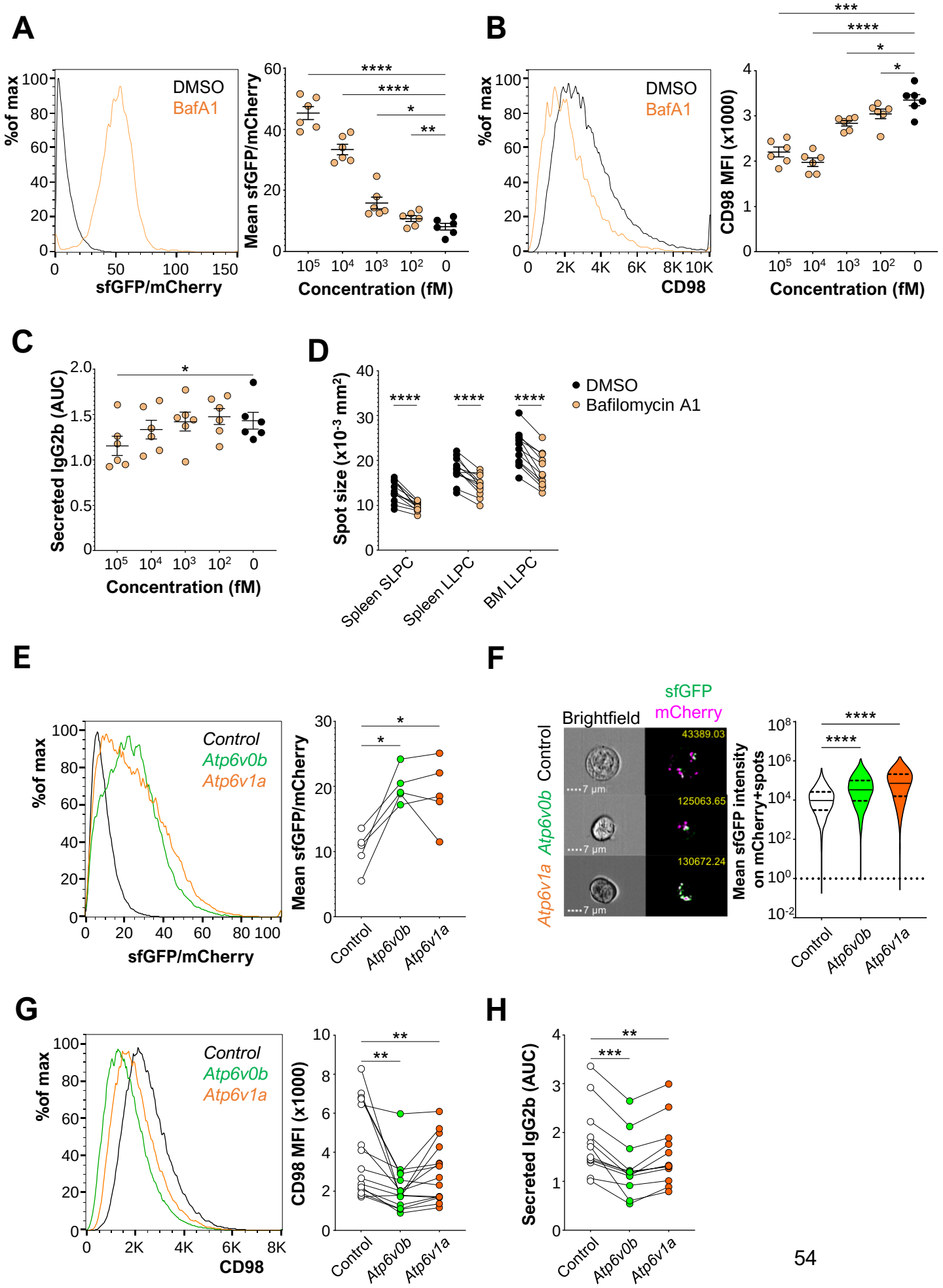
A
%of max
DMSO
BafA1
sfGFP/mCherry
Mean sfGFP/mCherry
Concentration (fM)
B
CD98
CD98 MFI (x1000)
C
Secreted IgG2b (AUC)
D
Spot size (x10⁻³ mm²)
Bafilomycin A1
Spleen SLPC
Spleen LLPC
BM LLPC
E
Control
Atp6v0b
Atp6v1a
F
Brightfield
sfGFP
mCherry
Mean sfGFP intensity on mCherry+spots
G
H

Fig. 5. V-type ATPase activity promotes CD98 expression and antibody secretion

(A) 5TGM1-Cas9-pHLARE cells were treated overnight with the indicated doses of Bafilomycin A1. Representative histogram of the ratio of sfGFP to mCherry MFI in DMSO (black) and 100nM Bafilomycin A1 (tan) treated groups (left). Quantification of mean sfGFP/mCherry ratio (right) in control and knockout cultures is shown. Pooled data from 6 experiments. *p<0.05 by Dunnett's multiple comparisons test.

(B) Cells in (A) were examined for MFI of surface CD98 by flow cytometry. Each circle represents the mean values for cells from a single well of an experiment. Pooled data from 6 experiments. *p<0.05 by Dunnett's multiple comparisons test.

(C) Culture supernatants of cells in (A) were scored for secreted IgG2b by ELISA. AUC for each group is shown. Pooled data from 6 independent experiments. *p<0.05 by Dunnett's multiple comparisons test.

(D) *Ex vivo* plasma cell subsets were sorted, and equal numbers were seeded into wells of an ELISpot plate containing media (untreated, black) or media with 10nM Bafilomycin A1 (tan). Quantification of average spot area of each subset in each treatment is shown. Each circle represents a single mouse and is connected across treatments with a line. Pooled data from 4 mice in a single experiment. *p<0.05 by two-way ANOVA.

(E) 5TGM1-Cas9-pHLARE cells were transduced with lentivirus containing gRNA targeting *Atp6v0b* or *Atpv1a* along with a control gRNA targeting the *Rosa26* locus. Representative histogram (left) of the ratio of sfGFP to mCherry MFI in control gRNA (black), *Atp6v0b*- (green), and *Atp6v1a*-targeting gRNA (orange) groups. Quantification of mean sfGFP/mCherry ratio (right) in control and knockout cultures. Each circle represents a single treatment and data points are joined by a line within the same

experiment. Pooled data from 5 independent experiments. *p<0.05 by Tukey's multiple comparisons test.

(F) Groups in (E) were assessed for sfGFP intensity on mCherry spots per cell by imaging flow cytometry. Representative images of each group (left) at 60x are shown with ratio values in the top right. Mean ratio of GFP intensity on mCherry+ spots/cell were quantified. Representative graph of 3 independent experiments. *p<0.05 by Games-Howell's multiple comparisons test.

(G) CD98 expression on 5TGM1-Cas9 cells transduced with control gRNA (black), *Atp6v0b*- (green), and *Atp6v1a*-targeting gRNA (orange). Representative histogram (left) and quantified CD98 MFI (right) depicted. Combined data from 15 experiments. *p<0.05 by Tukey's multiple comparisons test.

(H) Secreted IgG2b from culture supernatant of groups in (G) was quantified by ELISA. Area under the curve (AUC) for each group is shown. Pooled data from 12 experiments. *p<0.05 by Tukey's multiple comparisons test.

Figure 6

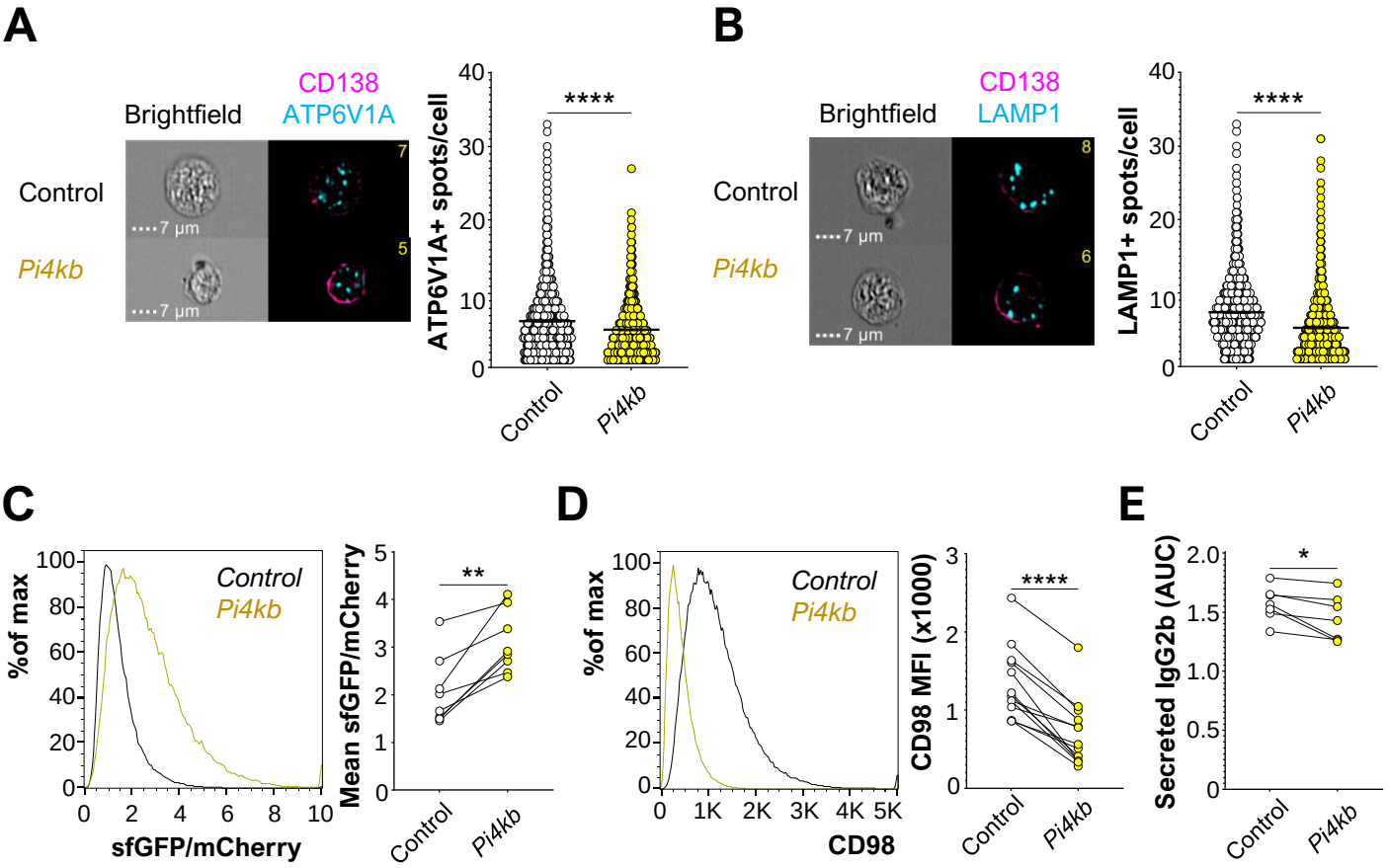
A
Brightfield
CD138
ATP6V1A
Control
Pi4kb
7 µm
7 µm
7
5
ATP6V1A+ spots/cell
****
Control
Pi4kb
B
Brightfield
CD138
LAMP1
Control
Pi4kb
7 µm
7 µm
8
6
LAMP1+ spots/cell
****
Control
Pi4kb
C
%of max
Control
Pi4kb
sfGFP/mCherry
Mean sfGFP/mCherry
**
Control
Pi4kb
D
%of max
Control
Pi4kb
CD98
CD98 MFI (x1000)
****
Control
Pi4kb
E
Secreted IgG2b (AUC)
*
Control
Pi4kb

Fig. 6. Ablation of *Pi4kb* reduces acidic vacuoles and antibody secretion

(A) 5TGM1-Cas9 cells transduced with control gRNA targeting the *Rosa26* locus (black) and *Pi4kb*-targeting gRNA (yellow) and then scored for intracellular ATP6V1A+ spots/cell. Representative images for each of the groups (left) and numbers of ATP6V1A+ spots/cell (right) were quantified. Pooled data from 4236-4368 cells across 3 independent experiments. *p<0.05 by an unpaired t-test with Welch's correction.

(B) Groups in (A) were scored for intracellular LAMP1+ spots/cell. Representative images for each of the groups (left) and numbers of LAMP1+ spots/cell (right) were quantified. Pooled data from 4830-4837 cells across 3 independent experiments. *p<0.05 by an unpaired t-test with Welch's correction.

(C) 5TGM1-Cas9-pHLARE cells were transduced with lentivirus containing gRNA targeting *Pi4kb* along with a control gRNA. Representative histogram (left) of the ratio of sfGFP to mCherry MFI in control gRNA (black) and *Pi4kb*-targeting gRNA (yellow) groups. Quantification of mean sfGFP/mCherry ratio (right) in control and knockout cultures. Each circle represents a single group and groups within the same experiment are joined by a line. Pooled data from 7 independent experiments. *p<0.05 by a paired t-test.

(D) Surface CD98 expression on groups in (C). Representative histogram (left) and quantified CD98 MFI (right) are shown. Combined data from 13 experiments. *p<0.05 by a paired t-test.

(E) Secreted IgG2b from culture supernatant of groups in (C) were quantified by ELISA. AUC for each group is shown. Pooled data from 7 experiments. *p<0.05 by a paired t-test.

Figure 7

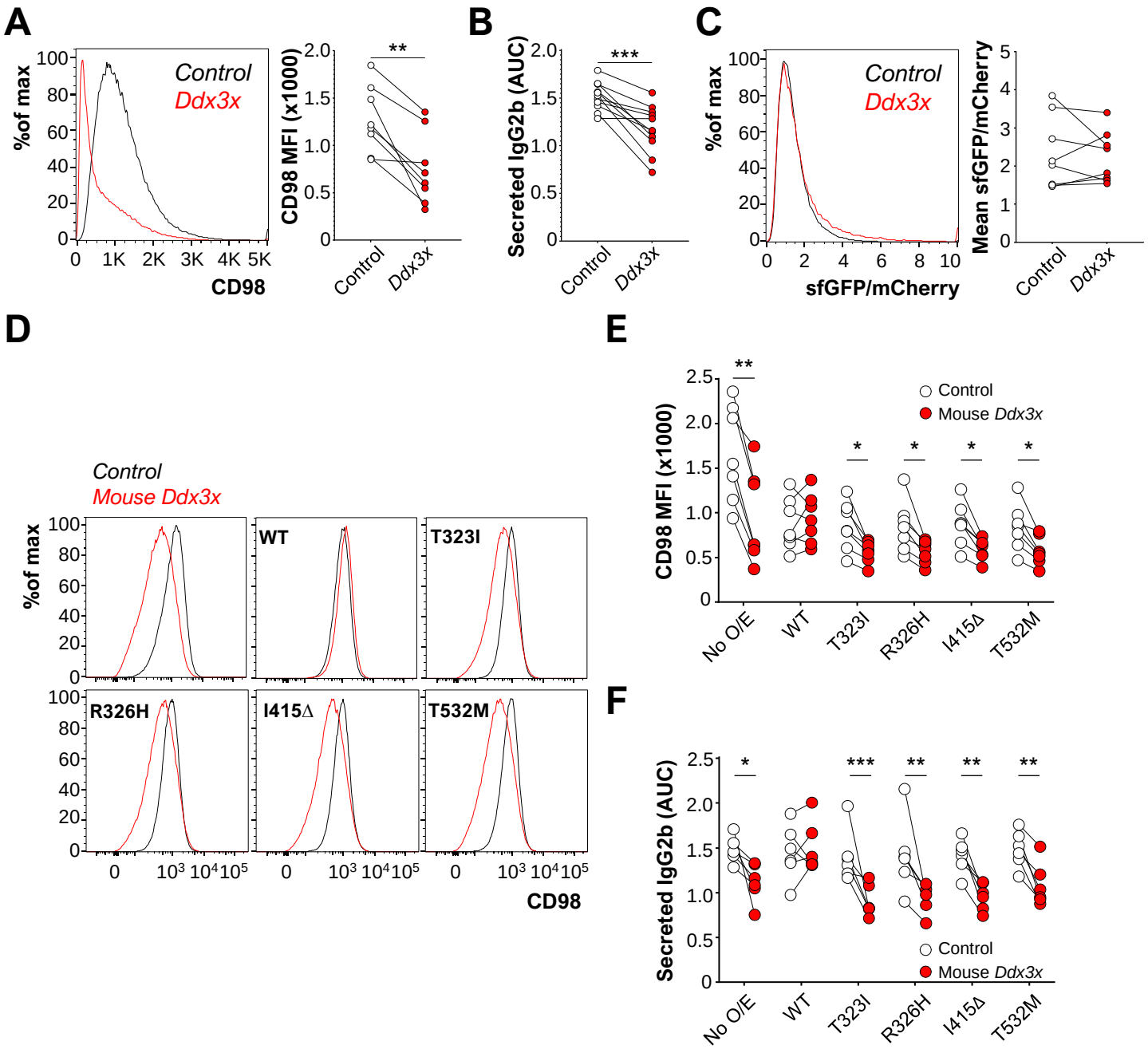
A
%of max
Control
Ddx3x
CD98
CD98 MFI (x1000)
Control
Ddx3x
B
Secreted IgG2b (AUC)
Control
Ddx3x
C
%of max
Control
Ddx3x
sfGFP/mCherry
Mean sfGFP/mCherry
Control
Ddx3x
D
Control
Mouse Ddx3x
%of max
WT
T323I
R326H
I415Δ
T532M
CD98
E
CD98 MFI (x1000)
Control
Mouse Ddx3x
No O/E
WT
T323I
R326H
I415Δ
T532M
F
Secreted IgG2b (AUC)
Control
Mouse Ddx3x
No O/E
WT
T323I
R326H
I415Δ
T532M

Fig. 7. DDX3X regulates antibody secretion independent of vacuolar acidification

(A) Surface CD98 expression on 5TGM1-Cas9 cells transduced with control gRNA targeting the *Rosa26* locus or gRNA targeting *Ddx3x*. Representative histogram (left) and quantified CD98 MFI (right) are shown. Combined data from 8 experiments. *p<0.05 by a paired t-test.

(B) IgG2b antibody levels in culture supernatants of cells in (C). AUC for each group is shown. Pooled data from 11 independent experiments. *p<0.05 by a paired t-test.

(C) 5TGM1-Cas9-pHLARE cells were transduced with lentivirus containing gRNA targeting *Ddx3x* as well as a control gRNA. Representative histogram (left) of the ratio of sfGFP to mCherry MFI in control gRNA (black) and *Ddx3x*-targeting gRNA (red) groups. Quantification of mean sfGFP/mCherry ratio (right) in control and knockout cultures is shown. Each circle represents a single group and groups within the same experiment are joined by a line. Pooled data from 8 experiments. No significance observed by a paired t-test.

(D) 5TGM1-Cas9 cells overexpressing hsDDX3X or catalytically inactive hsDDX3X mutants were transduced with control gRNA or gRNA targeting mouse *Ddx3x*. Representative histograms for surface CD98 distribution on cells transduced with control gRNA (black) and mouse *Ddx3x* (red) are shown for cells without overexpression (top left), cells overexpressing WT DDX3X (top center), and cells overexpressing indicated mutant DDX3X (remaining squares).

(E) Quantification of surface CD98 expression on cells in (D) as well as cells overexpressing DDX3X mutants. Pooled data from 6 independent experiments. *p<0.05 by Sidak's multiple comparisons test.

(F) Culture supernatants of all groups in (E) were assessed for secreted IgG2b by ELISA. AUC for each group is shown. Pooled data from 6 experiments. *$p<0.05$ by Sidak's multiple comparison test.

Figure 8

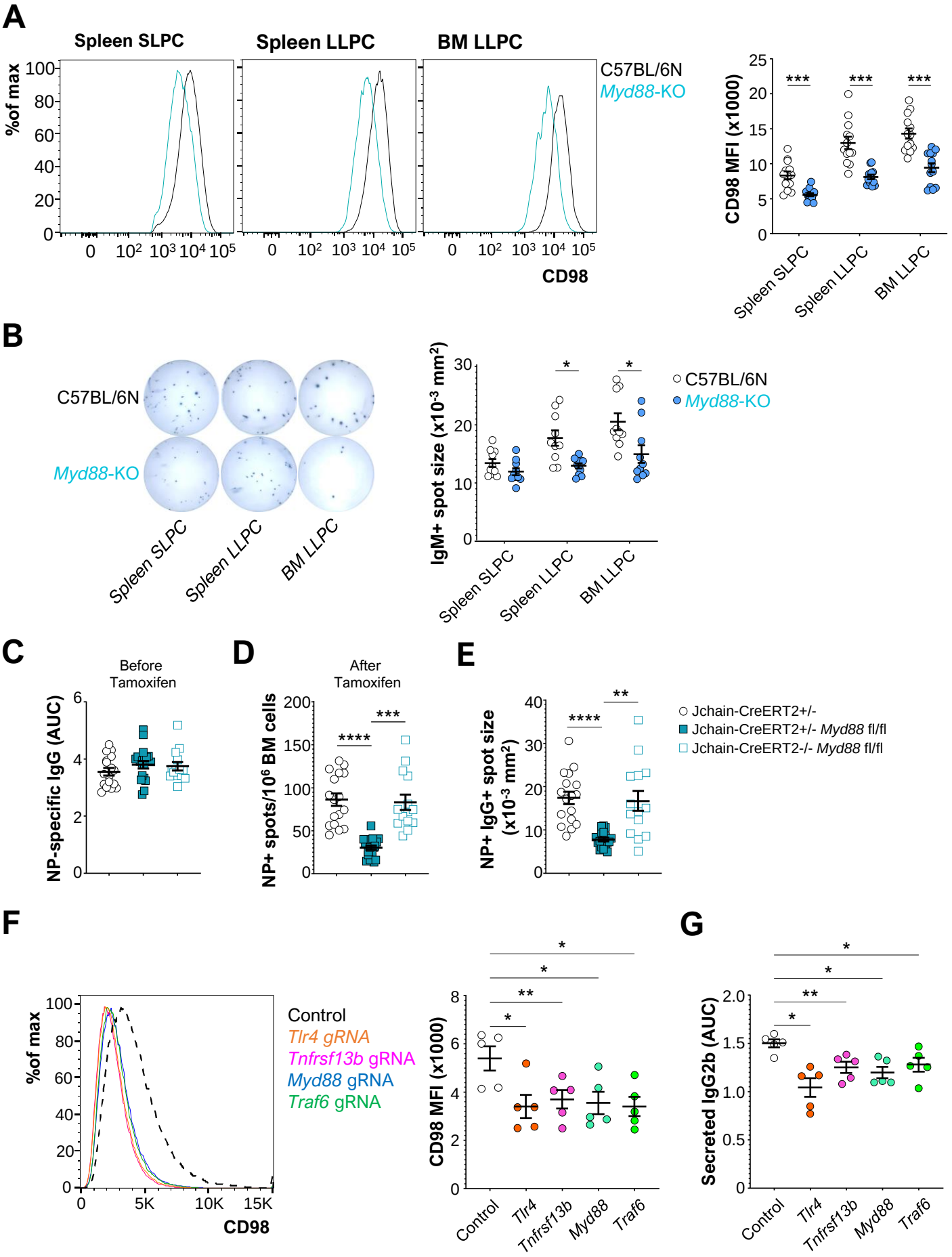
A
Spleen SLPC
Spleen LLPC
BM LLPC
%of max
C57BL/6N
Myd88-KO
CD98
CD98 MFI (x1000)
B
C57BL/6N
Myd88-KO
Spleen SLPC
Spleen LLPC
BM LLPC
IgM+ spot size (x10-3 mm2)
C
Before Tamoxifen
NP-specific IgG (AUC)
D
After Tamoxifen
NP+ spots/106 BM cells
E
NP+ IgG+ spot size (x10-3 mm2)
Jchain-CreERT2+/-
Jchain-CreERT2+/- Myd88 fl/fl
Jchain-CreERT2-/- Myd88 fl/fl
F
Control
Tlr4 gRNA
Tnfrsf13b gRNA
Myd88 gRNA
Traf6 gRNA
CD98 MFI (x1000)
G
Secreted IgG2b (AUC)
Control
Tlr4
Tnfrsf13b
Myd88
Traf6

Fig. 8. Plasma cell intrinsic MYD88 promotes antibody secretory capacity and longevity

(A) Representative histograms of surface CD98 levels on IgM+ splenic SLPCs (left), splenic LLPCs (center), and bone marrow LLPCs (right) from C57BL/6N (black) and *Myd88*-KO mice (blue). CD98 MFI was then quantified on indicated groups. Each circle is representative of a single mouse. Pooled data from 13 mice of each genotype across 4 independent experiments. *p<0.05 by Sidak's multiple comparisons test.

(B) Indicated IgM+ plasma cell populations were purified from the spleens and bone marrows of C57BL/6N (black) and *Myd88*-KO mice (blue) and seeded into an ELISpot plate. Representative images showing spots from indicated plasma cell subset from indicated mice are shown (left). Spot sizes of IgM-secreting plasma cells are quantified (right). Combined data from 10 mice across 3 experiments. *p<0.05 by Sidak's multiple comparisons test.

(C) Serum NP-specific IgG levels in Jchain-CreERT2+/- (black, filled circles), Jchain-CreERT2+/- *Myd88* fl/fl (blue, filled squares), and Jchain-CreERT2-/- *Myd88* fl/fl (blue, open squares) at 8 weeks post immunization with NP-CGG in Alhydrogel. Pooled data from 14-20 mice per group across 3 different experiments. No statistical significance observed by Dunnett's T3 multiple comparisons test.

(D) Mice in (C) were placed on tamoxifen chow for 14 days. CD138+ bone marrow cells were enriched and seeded into an ELISpot plate. Numbers of NP-specific IgG+ spots per million cells are quantified and represented. *p<0.05 by Dunnett's T3 multiple comparisons test.

(E) NP-specific IgG spot sizes in (D) were quantified and shown. *p<0.05 by Dunnett's T3 multiple comparisons test.

(F) 5TGM1-Cas9 cells were transduced with gRNA targeting *Tlr4*, *Tnfrsf13b*, *Myd88*, or *Traf6*. Representative histograms (left) showing surface CD98 levels in transduced groups (colored) relative to control gRNA transduced cells (black dashed). CD98 MFI (right) was quantified across 5 independent experiments. *p<0.05 by Dunnett's multiple comparisons test.

(G) Secreted IgG2b from culture supernatant of groups in (F) were quantified by ELISA. AUC for each group is shown. Pooled data from 5 experiments. *p<0.05 by Dunnett's multiple comparisons test.

Supplementary Figure 1

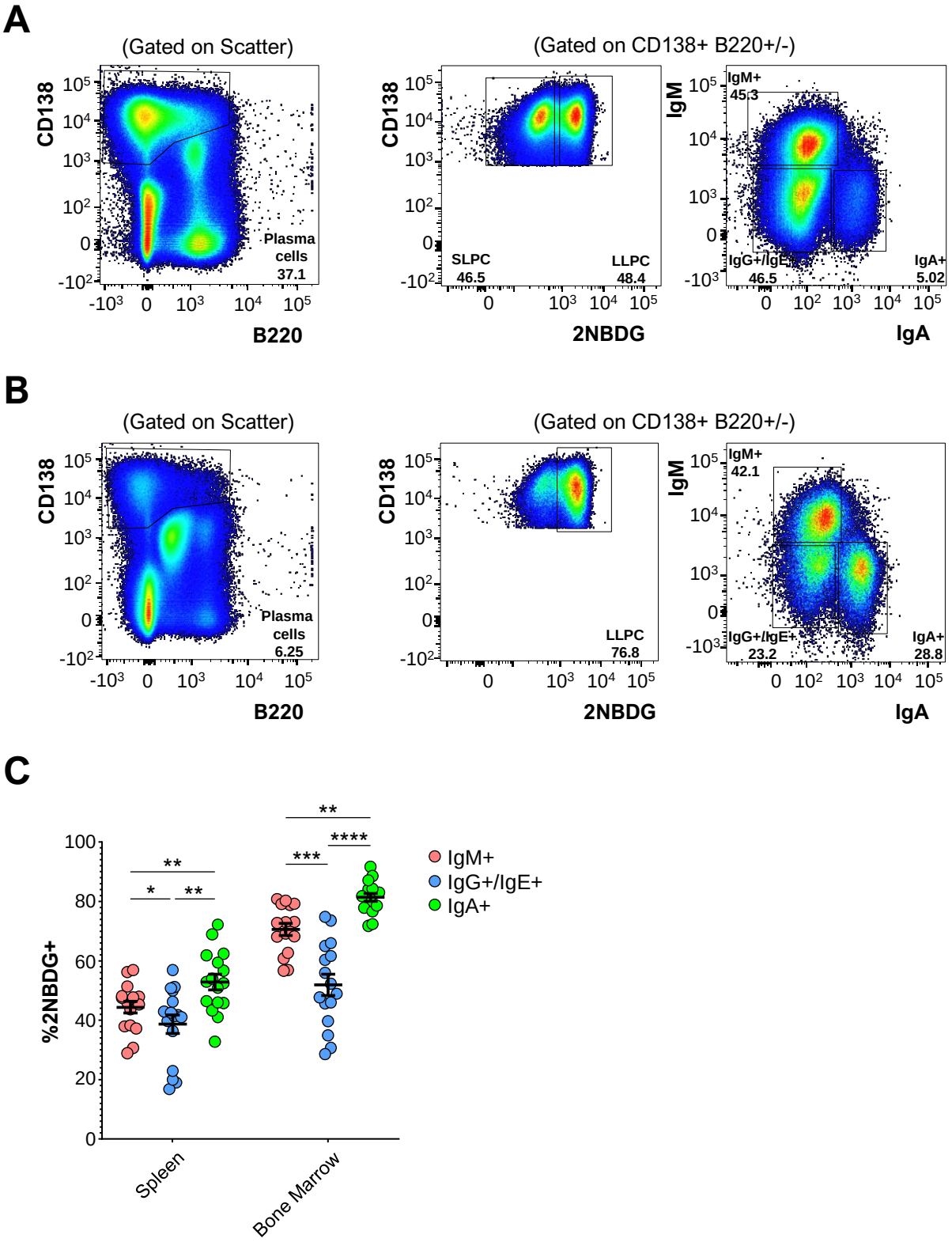

Supplementary Fig. 1. Murine plasma cell subsets have disparate proportions of 2NBDG+ cells.

(A) Representative gating of mouse splenic plasma cells on enriched CD138+ splenocytes. Single cells were gated first as CD138+ B220+/- cells (left) and then distinguished as 2NBDG- SLPC and 2NBDG+ LLPC (center), IgM+, IgA+, or IgG+ and IgE+ (right).

(B) Representative gating of murine bone marrow plasma cell subsets gated as in (A).

(C) Long lived plasma cell frequencies as defined by 2NBDG uptake in mouse splenic and bone marrow IgM+, IgG+ and IgE+, and IgA+ plasma cells. Pooled data from 16 mice across 4 experiments.

Supplementary Figure 2

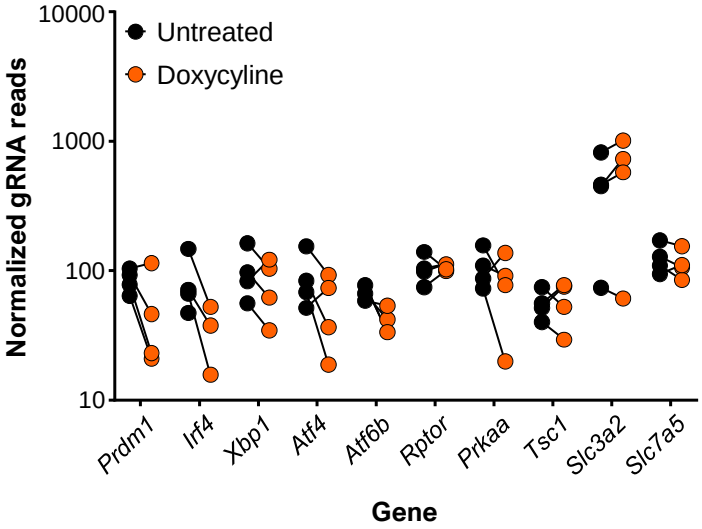

Supplementary Fig. 2. Cas9 induction leads to reduced abundance of gRNAs targeting essential genes in 5TGM1-iCas9-Brie cultures

5TGM1-iCas9-Brie cells were left untreated or treated with Doxycycline. At day 7, gRNA abundance was quantified from both groups using MaGeCK. Normalized counts of gRNA targeting indicated genes are shown in both groups. Matching gRNAs are connected by a line. Pooled data from 4 biological replicates.

Supplementary Figure 3

A

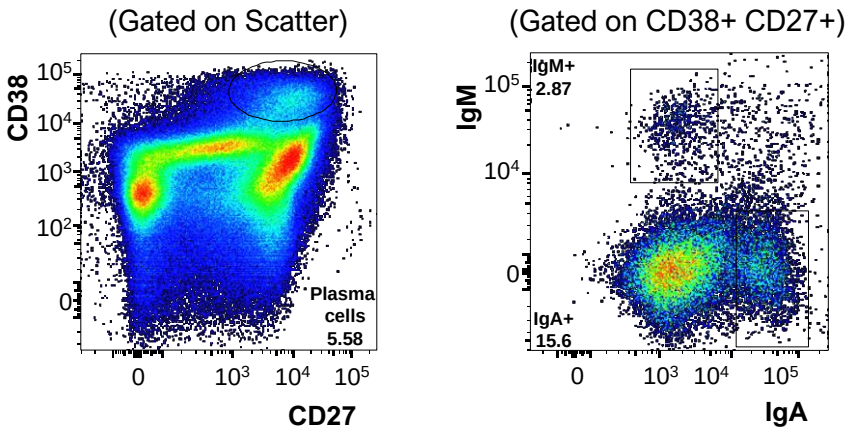

B

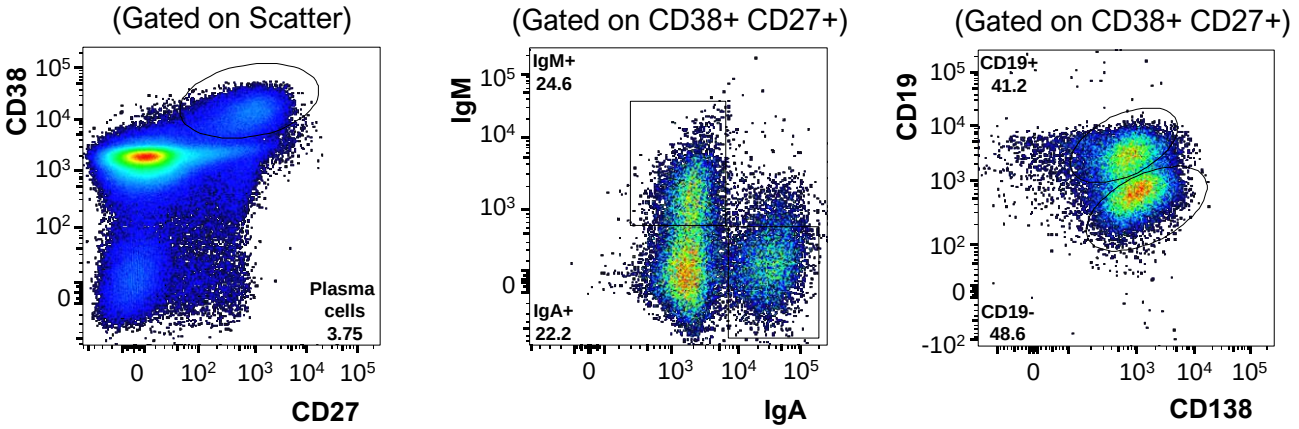

Supplementary Fig. 3. Identification of human plasma cell subsets

(A) Representative gating of human tonsil plasma cells on CD38+ enriched cells. Cells were identified as CD38+ CD27+ cells on single cells (left). Cells were then identified as IgM- or IgA-secretors based surface expression of the respective isotype (right). Double negative cells were presumed IgG+ and IgE+ plasma cells.

(B) Bone marrow plasma cells of various isotypes were gated like tonsillar plasma cells as CD38+ CD27+ single cells (left, center). Human plasma cell subsets were then identified as CD138+ CD19+ or CD138+ CD19- cells respectively (right).

Supplementary Figure 4

A

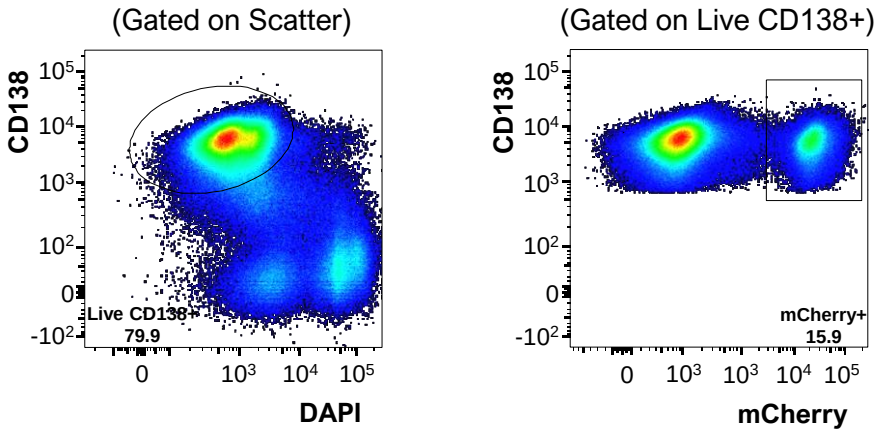

B

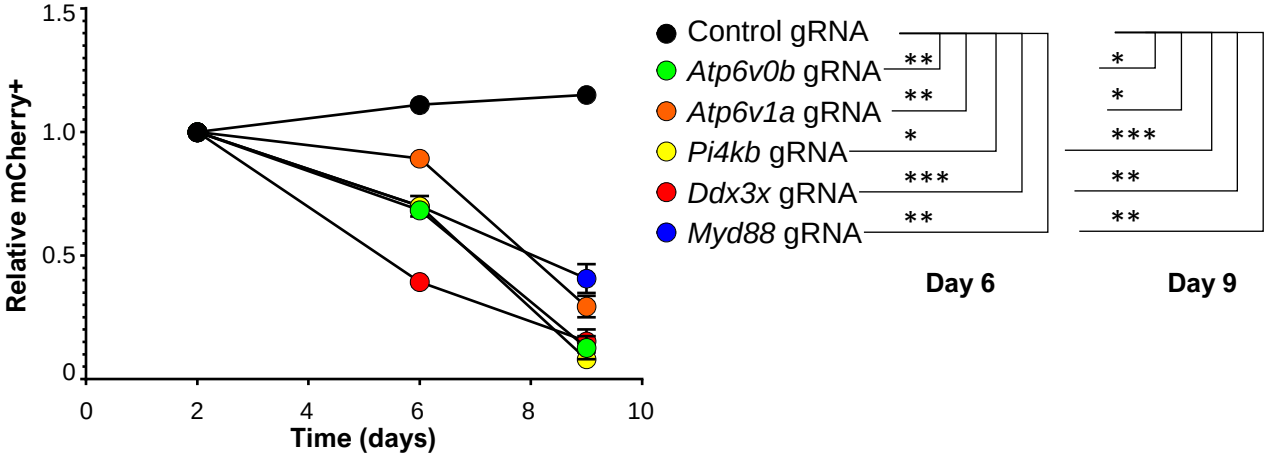

Supplementary Fig. 4. Perturbations in *Atp6v0b*, *Atp6v1a*, *Pi4kb*, *Ddx3x*, and *Myd88* compromise cell survival

(A) 5TGM1-Cas9 cells were transduced with lentivirus containing lentiGuide-mCherry with control gRNA targeting the *Rosa26* locus or gRNA targeting *Atp6v0b*, *Atp6v1a*, *Pi4kb*, *Ddx3x*, and *Myd88*. Representative flow cytometry plots depicting live myeloma cells (left) at day 2 post transduction with mCherry+ frequencies on them (right).

(B) Transduced cells in (A) were tracked in culture over time and mCherry+ frequencies measured at days 2, 6, and 9 after transduction. mCherry+ frequencies were normalized to frequencies at day 2. Statistical significance for each group relative to the control was calculated and indicated in the figure legend for day 6 and day 9. *$p<0.05$ by two-way ANOVA.

Supplementary Figure 5

A

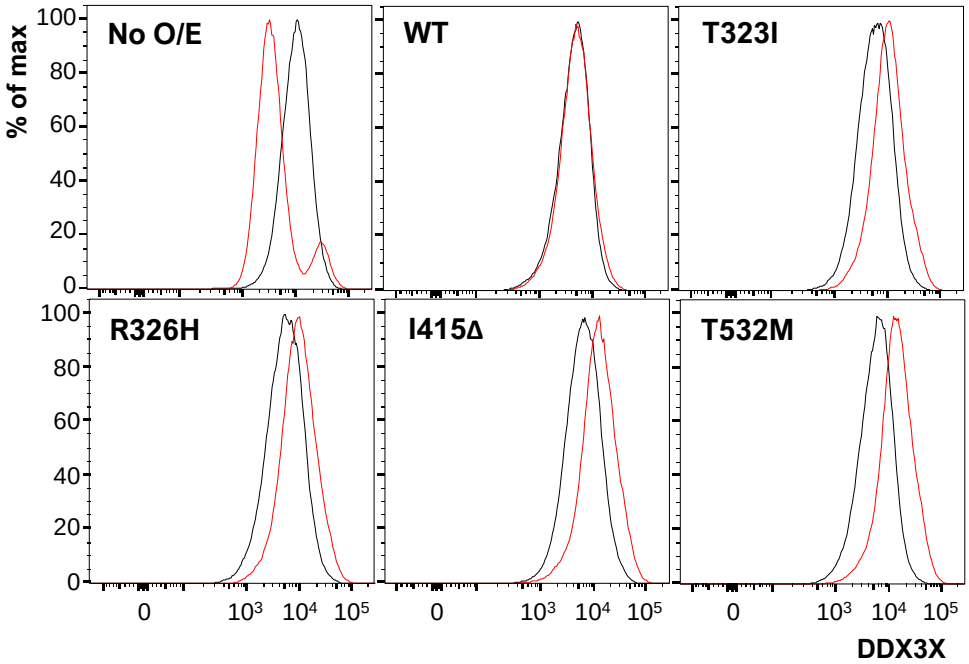

B

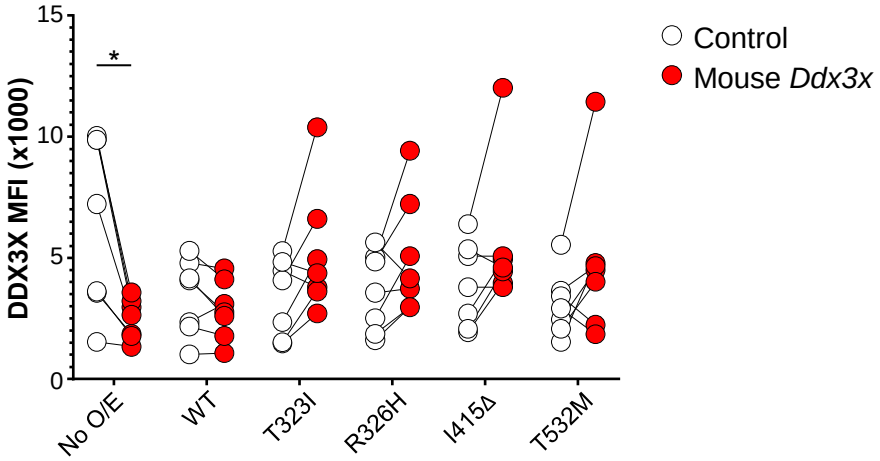

Supplementary Fig. 5. DDX3X protein levels are comparable in overexpression cultures after ablation of endogenous mouse DDX3X.

(A) 5TGM1-Cas9 cells overexpressing human DDX3X proteins were transduced with gRNA targeting mouse *Ddx3x* (red) or control gRNA targeting the *Rosa26* locus (black). Cells not overexpressing DDX3X are shown on the top left. Representative histograms are shown for each of the groups.

(B) Quantification of the MFI of various groups in (A) are displayed. Each line connects groups within the same experiment. Pooled data from 7 independent experiments. *$p<0.05$ by Sidak's multiple comparisons test.

Supplementary Figure 6

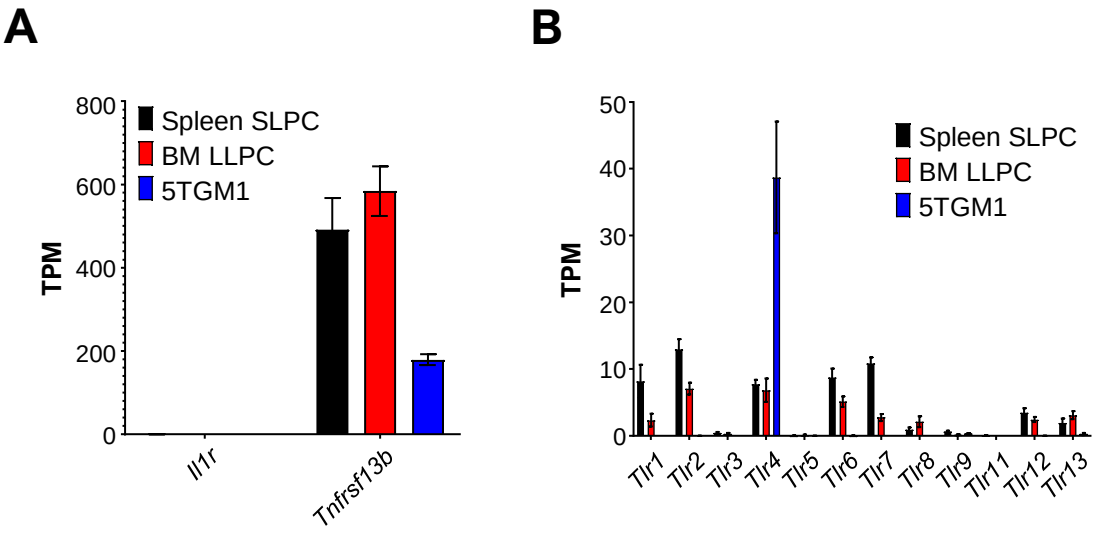

Supplementary Fig. 6. Plasma cell subsets express TACI and multiple TLRs but not IL-1R.

(A) TPM values of IL-1R (*Il1ra*) and TACI (*Tnfrsf13b*) showing data from splenic and bone marrow plasma cell subsets from Lam WY *et al* (Cell Reports 2018) and 5TGM1 cells from D'Souza L *et al*, (PLoS One 2022). Pooled data from three independent experiments.

(B) TPM values of members of the TLR family of genes are shown for populations mentioned in (A). Pooled data from three independent experiments.